Instituto Tecnológico y de Estudios Superiores de Monterrey

Campus Monterrey

School of Engineering and Sciences

Relationship between physical and acoustical parameters for road surface characterization

A thesis presented by

Jesús Rodrigo Leos Suárez

Submitted to the

School of Engineering and Sciences
in partial fulfillment of the requirements for the degree of

Master of Science

In

Manufacturing Systems

Monterrey, Nuevo León, December 04th, 2018

Instituto Tecnológico y de Estudios Superiores de Monterrey

Campus Monterrey

School of Engineering and Sciences

The committee members, hereby, certify that have read the dissertation presented by Jesús Rodrigo Leos Suárez and that it is fully adequate in scope and quality as a partial requirement for the degree of Master of Science in Manufacturing Systems.

Dr. Alex Elías Zúñiga
Tecnológico de Monterrey
Advisor

Dr. David Isaac Ibarra Zárate
Tecnológico de Monterrey
Co-advisor

M.Sc. Christian Carrillo Vasquez
IKA-RWTH Aachen University
Committee Member

Tecnológico de Monterrey
04 DIC 2018
Dirección Nacional de Posgrado
Dr. Rubén Morales Menéndez

Dra. Luz María Alonso Valerdi
Tecnológico de Monterrey
Committee Member

Dr. Oscar Martínez Romero
Tecnológico de Monterrey
Committee Member

Dr. Rubén Morales Menéndez
Dean of Graduate Studies
School of Engineering and Sciences

Monterrey, Nuevo León, December 04th, 2018

Declaration of Authorship

I, Jesús Rodrigo Leos Suárez, declare that this dissertation titled, "*Relationship between physical and acoustical parameters for road surface characterization*" and the work presented in it are my own. I confirm that:

- This work was done wholly or mainly while in candidature for a research degree at this University.
- Where any part of this dissertation has previously been submitted for a degree or any other qualification at this University or any other institution, this has been clearly stated.
- Where I have consulted the published work of others, this is always clearly attributed.
- Where I have quoted from the work of others, the source is always given. With the exception of such quotations, this dissertation is entirely my own work.
- I have acknowledged all main sources of help.
- Where the dissertation is based on work done by myself jointly with others, I have made clear exactly what was done by others and what I have contributed myself.

Jesús Rodrigo Leos Suárez
Monterrey, Nuevo León
December 4th 2018

@2018 by Jesús Rodrigo Leos Suárez
All rights reserved

Dedication

To God, for allowing me to reach this stage of my life and give me the courage to keep going.

To my family, who taught me that roads are formed, that life is not easy, but that there are always solutions. That fate is not expected but reached.

To you who formed me with love, repeating with hugs that I could be, who I wanted to be, that I could achieve everything, if I make an effort to do so.

To you who taught me to enjoy the present, but to look forward to the future. That a failure, it is just a new opportunity to start over.

To you, who with your experience, support, understanding and dedication, plant in me the healthy ambition to achieve this goal, which ends today.

To you all, THANK YOU.

Acknowledgements

I would like to express my deepest gratitude to Dr. David Ibarra for all his dedication and orientation, but specially for his friendship.

To my family, for their continuous motivation and support through all the process to make this and all my goals possible.

To my best friends Iván Vázquez, Gerardo Maycotte, Daniel Rimada and Mauricio Pérez, with great admiration to you all.

To my fellow students and friends Oscar Jesús Escalera, José Alberto Robles, Javier Sierra, Sergio Alahudy, Jorge Islas, Pedro Vázquez, José Luis Padilla and Alan Pérez for all being part of a supporting group with the best hopes even at difficult times.

The project in collaboration with the Institute for Automotive Engineering in Aachen (IKA), but specially to M. Sc. Christian Carrillo for giving me the opportunity to work together in mutual projects and gaining experience from very interesting automotive research projects.

And finally, I want to thank Tecnológico de Monterrey for the current support tuition, with almost 10 years of my life studying at this great institution, and CONACYT for the maintenance support during the last 2 years.

Relationship between physical and acoustical parameters for road surface characterization

By
Jesús Rodrigo Leos Suárez

Abstract

An acoustic system for automated road surface conditions detection from acoustic signals of surface interaction is introduced. The aim of this work is to obtain different characteristics of the roadway surface by which the vehicle is circulating, to analyze its texture, friction and other characteristics related to the road surface with anticipation so that this information could be used in future automotive safety applications. The advantages of using an acoustic device compared with other current technologies is the low cost of the equipment and its portability.

The robustness of our approach is evaluated on audio that span an extensive range of vehicle speeds, noises from the environment, road surface types, and pavement conditions including international friction index (IFI) values from 0 km/hr to 100 km/hr. The training and evaluation of the model were performed on different roads to minimize the impact of environment and other external factors on the accuracy of the classification. The results showed that there is a correlation between what we measured with the mechanical systems and what we obtained as a reply from the acoustic system.

The hypothesis is that with the application of an acoustic device that characterizes the pavement in real time, future automotive applications such as adjusting the ABS system automatically in an optimal range of braking, showing a warning indicator light on the dashboard, or improving the driving decision making of autonomous cars will be possible by having prior information of the slippery surface conditions in which the vehicle transits.

List of Figures

Figure 1 - Passenger vehicle with all-season tires: Approximate stopping distance in meters. Modified from [7] 2
Figure 2 - Typical conformation of a flexible pavement. 8
Figure 3 - Typical conformation of a rigid pavement. 8
Figure 4 - Schematic Plot of Hysteresis and Adhesion 10
Figure 5 - Influence of the range of surface irregularities in the phenomena of interaction between vehicles and the road. [12] 12
Figure 6 – Example of equipment used to characterize asphalt 13
Figure 7 - British friction pendulum (ASTM E 274) 14
Figure 8 – Schematic of British Pendulum tester 15
Figure 9 – Sand patch test (ASTM E 965) 17
Figure 10 - Interpretation areas of the diagram Friction vs. Macrotexture [15] 21
Figure 11 - Wave vector **K0** incident to a surface containing cylinders of radius a and mean center-to-center spacing b [37]. 22
Figure 12 - Wave vector **K0** incident to a rough surface ξ 23
Figure 13 - Geometry to study the attenuation between source and receiver in presence of a porous ground formed with several absorbent layers 24
Figure 14 - A plane wave incident on a homogeneous medium. 26
Figure 15 - Experimental setup. 27
Figure 16- Experimental difference curves at different speeds with noise filtered. .. 28
Figure 17- Theoretical and experimental level difference curves for the asphalt at 100 km/h. 29
Figure 18 - Comparison chart of flow resistivity, porosity and shape factor at 0 and 100 km/h 30
Figure 19– Location of measurements around the ITESM – Campus Monterrey 31
Figure 20 – Friction measurement at 1st location 32
Figure 21– Macrotexture measurement at 3th location 33
Figure 22 - Comparison of sections with IFI (F60, Sp) 34
Figure 23 – Acceptance/Rejection curve for the five locations 35
Figure 24 – Static system 37
Figure 25 – Acoustic measurement at the 1st location 37
Figure 26 - Comparison of flow resistivity for 1 to 4 parameters 39
Figure 27 - Comparison of porosity for 3 and 4 parameters 39
Figure 28 - Comparison of tortuosity for 3 and 4 parameters 39
Figure 29- Representation of the acoustic system mounted on the car 40
Figure 30 - Acoustic system mounted at the front of the driver's rear tire 40
Figure 31 - Comparison of flow resistivity for 1 to 4 parameters 42

Figure 32 - Comparison of porosity for 3 and 4 parameters 42
Figure 33 - Comparison of tortuosity for 3 and 4 parameters 42
Figure 34 - Correlation between IFI and Porosity with 3 parameters. (r=0.26) 44
Figure 35 - Correlation between IFI and Porosity with 4 parameters. (r=0.25) 44
Figure 36 - Correlation between IFI and Porosity with 3 parameters (r=-0.85) 45
Figure 37 - Correlation between IFI and Porosity with 4 parameters (r=-0.27) 45
Figure 38 - Correlation between Friction and Porosity with 3 parameters (r=-0.42) 46
Figure 39 - Correlation between Friction and Porosity with 4 parameters (r=-0.5) .. 46
Figure 40 - ABS System. 49
Figure 41 - Braking slip effect on friction coefficient vs. wheel slip 49
Figure 42 - Work flow of the implementation. 50
Figure 43 – Elements of an Anti-Lock Braking System (ABS) model 50
Figure 44 – Slippery Condition Warning 51
Figure 45– Automated driving system 51
Figure 46 - Correction factor for temperature. 60
Figure 47 - Matlab Graphical User Interface (GUI) 63
Figure 48 – Theoretical and experimental level difference curves for the asphalt at 20 km/h 64
Figure 49 - Theoretical and experimental level difference curves for the asphalt at 100 km/h 65
Figure 50 - Layer of fluid. 68
Figure 51 - Layer of fluid backed by a rigid wall 69
Figure 52 – Sample tests divided by percentage of asphalt 76-22. 72
Figure 53 - British pendulum measurement experimentation 73
Figure 54 – Analysis of measurements using MATLAB 73
Figure 55 – Acoustic absorption comparison between 700-1100 Hz 74
Figure 56 – Friction vs Ac. Absorption for 700 Hz 75
Figure 57 – Friction vs Ac. Absorption for 800 Hz 75
Figure 58– Friction vs Ac. Absorption for 900 Hz 76
Figure 59 – Friction vs Ac. Absorption for 1000 Hz 76
Figure 60 – Friction vs Ac. Absorption for 1100 Hz 76
Figure 61 - Impedance tube configuration I: microphone A in position 1 and microphone B in position 2. 79
Figure 62 - Impedance tube configuration II: microphone B in position 1 and microphone A in position 2. 79
Figure 63 – Example of microphone assembly. [49] 81
Figure 64 – Example of system assembly. [49] 81

List of Tables

Table 1 – Factors affecting pavement friction. Modified from [53] 10
Table 2 - Classification of surface irregularities of a pavement (flexible or rigid). .. 11
Table 3 - Microtexture values proposed by the Mexican government. [17] 16
Table 4 - Macrotexture values proposed by the Mexican government. [17] 18
Table 5 - Surface parameters obtained at different speeds. 29
Table 6 – Friction values measured with the British pendulum on road surfaces 32
Table 7 – Sand patch test measurements (mm) 33
Table 8 – Calculation of IFI 34
Table 9 – Acoustic parameters measured with static system 38
Table 10 – Acoustic parameters measured with dynamic system 41
Table 11 – Static system correlation coefficient (r) comparison. 43
Table 12 – Dynamic system correlation coefficient (r) comparison. 45
Table 13 – Granulometry of experimental tests per batch 71
Table 14 – Asphalt 76-22 test sample properties 71
Table 15 - Friction values measured with the British Pendulum on test samples 73
Table 16 – Acoustic absorption (α) values for different frequencies 74
Table 17 – Acoustic vs. Friction correlation coefficient for different frequencies 77

Contents

Abstract viii

List of Figures ix

List of Tables xi

Chapter 1 Introduction 1

1.1 Motivation 1

1.2 Problem Statement 1

1.3 Research Questions 2

1.4 Solution Overview 3

1.5 Main Contribution 3

1.6 Dissertation Organization 3

Chapter 2 Framework 5

2.1 Literature Review 5

2.2 Theoretical Background 6

2.3 Types of pavements in Mexico 7

2.3.1 Flexible pavements 7

2.3.2 Rigid pavements 8

2.4 Tire-Road Interaction 9

2.4.1 Factors Affecting Pavement Friction 10

2.4.2 Pavement Surface Characteristics 11

Chapter 3 System Design 13

3.1 Mechanical characterization of pavement surface 13

3.1.1 Differentiation of equipment 13

3.1.2 British Pendulum Test (Microtexture) 13

3.1.3 Sand Patch Test (Macrotexture) 16

3.1.4 International Friction Index 18

3.2 Acoustic parameters of road surface 21

3.2.1 Modeling of random ground roughness effect by an effective impedance 21

3.2.2 Theoretical model of acoustic system proposal 24

3.2.3 Experimental methodology based on previous work 27

Chapter 4 Methods 31

4.1 Measurements with Mechanical Equipment 31

4.1.1 Friction measurement with British Pendulum Test 31

4.1.2 Macrotexture measurement with Sand Patch Test 32

4.1.3 International Friction Index 33

4.1.4 Acceptance/Rejection Graph 35

4.2 Measurement with Acoustic System 36

4.2.1 Description 36

4.2.2 Static Measurements 37

4.2.3 Dynamic Measurements 40

Chapter 5 Results **43**
5.1 Relationship between mechanical and acoustical parameters **43**
5.1.1 Static Measurements 43
5.1.2 Dynamic Measurements 44
Chapter 6 Conclusions **47**
6.1 Contributions **47**
6.2 Future work **48**
Bibliography **52**
Abbreviations and Acronyms **57**
Variables Descriptions and Symbols **58**
Appendix A **59**
A.1 British Pendulum **59**
A.2 Sand patch **60**
Appendix B GUI of Data Acquisition System **63**
Appendix C Impedance Tube **66**
Appendix D Experimentation with Impedance tube **71**
D.1 Granulometric composition of experimental samples **71**
D.2 Experimental Measurements **72**
D.2.1 British Pendulum 72
D.2.2 Impedance Tube 73
D.3 Results **74**
D.4 Discussion **77**
Appendix E Calibration of impedance tube measurement setup **78**
Annex A Construction of the Impedance tube **81**
Curriculum Vitae **82**

Chapter 1

Introduction

1.1 Motivation

An acoustic system for automated road surface conditions detection using acoustic signals of surface interaction is explained. The aim of this work is to obtain different characteristics of the roadway surface on which the vehicle is circulating by analyzing friction and texture with anticipation to either improve the dynamic systems of the vehicle or create a mapping of unsafe roads.

The use of audio to road condition automated detection may have some important potential applications for the automotive safety systems. Some of the applications may be to give these road conditions as an additional input value to the Antilock Braking System (ABS), or to the next generation Advanced Driver Assistance Systems (ADAS) that have the potential to enhance driver safety, or to the autonomous vehicles that have to be aware of road conditions to automatically adapt vehicle speed while entering the curve or keep a safe distance to the vehicle in front. [1]

Nowadays, there are different approaches to detect weather surface conditions, but in most of cases they are not robust to variation in real-world datasets. The use of video-based wetness prediction for example is limited when poor lighting conditions are present, which could be the case at night or when fog and smoke are present. The measurements with our audio-based characteristics prediction dataset are heavily dependent upon surface type and vehicle speed. [2]

1.2 Problem Statement

Nowadays, great technological advances are focused on the automotive industry, where cars are constantly improving in autonomy and safety. Safety represents an important issue for the automotive companies, at first, passive safety systems as for example seat belts and airbags were implemented in the vehicles. These passive systems protect the passengers in the case of an accident. However, the recent implementation of active safety systems is used to prevent any kind of accident by predicting it before it happens. An example of an active safety system is the Anti-Lock Braking System (ABS) [3].

When an action of panic braking exists, the driver applies a force over the braking pedal and the car starts rapidly decelerating until the steady state, which produces a tire lock in comparison with the ground, losing the complete control and direction of the vehicle. The explanation of this fact is that the brake prevents the wheel from spinning provoking it to slide,

especially when the coefficient of friction between the wheels and the ground is low, and in this case, the stability control of the vehicle is lost. The Anti-Lock Braking System helps avoiding this kind of situations by maintaining the vehicle slip between desired ranges, but even though, a total control of the system by knowing the coefficient of friction with anticipation to feedback the system has not yet been developed.

According to the latest National Institute of Statistics and Geography (INEGI) report from 2017 [4], 367,789 car accidents were registered in Mexico, of which 91,157 were people injured and 4,394 died. This generates a total of nearly 11,000 accidents due to bad conditions of the paved road surface annually in Mexico. With this information, it is obviously shocking to see the number of people that are affected by the problem. For this case, it is necessary to develop a system that can determine the characteristics of the roadway surface through which the vehicle transits. To this purpose, it is necessary to identify possible options for measuring the characteristics of the roadway surface by which the vehicle is circulating, to feed the data of the measurements in real time with the dynamic systems of the vehicle, so that these adjust the ABS system automatically.

It has been suggested that the braking distances vary greatly on the type of tire, speed and road conditions, as seen in Figure 1 [5]. Self-driving cars must identify wet/dry road conditions on the fly and adjust to the safe following distance. Braking distance for wet road is 30-40% longer than the braking distance for dry road, while the real distance greatly depends on clear visibility, mental workload and many other factors [6].

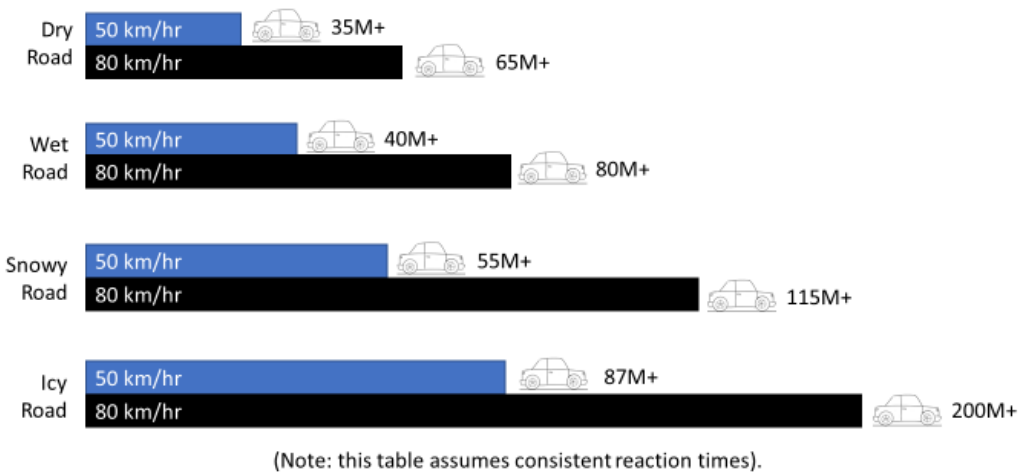

Figure 1 - Passenger vehicle with all-season tires: Approximate stopping distance in meters. Modified from [7]

1.3 Research Questions

Is there a relationship between the mechanical and acoustical systems for road characterization? And if so, is there any direct relationship between the road surface friction coefficient and the acoustic absorption coefficient? and finally, could we communicate this prior information as an input value to the Anti-lock Braking System (ABS) or any other

assistance system of the car to prevent an accident regarding the road surface?

Mechanical systems already characterize road surfaces. The aim of this thesis is to correlate and use an acoustical system with the same purpose, in order to have a portable system on the car to measure the road surface characteristics in real time.

Until now there are no similar system, so a challenge of the work is to validate the audio-based systems.

1.4 Solution Overview

The hypothesis is that with the application of an acoustic device that characterizes the pavement in real time, we will improve the response time and performance of either the ABS, ADAS or the autonomous vehicles, because the system would be controlled by having prior information of the slippery surface conditions to automatically adapt, or to give a warning information to the driver.

The acoustic system works by emitting sounds with a speaker and evaluating the received difference of pressure between two microphones at different levels. The difference between the direct and the reflected sound pressure has to do with the ground absorption of the sound wave.

Some of the mechanical equipment used in the experimentation were both British pendulum to measure friction conditions, and the Sand patch test to measure macrotexture conditions.

Based on this procedure, it is intended to correlate mechanical properties of the road such as friction and macrotexture with acoustical properties such as porosity, flow resistivity, tortuosity and shape factor.

1.5 Main Contribution

The contribution of the acoustic system is to know, in real time, the physical parameters of road surface measured, minimizing the influence of aerodynamic noise. The low cost and its portability make the system to be a very useful tool for noise predictions in outdoors propagation and could be used as a complement instrument in noise mapping.

1.6 Dissertation Organization

This research work is organized as follows:

- Chapter 2 presents the state of the art of different approaches for road surface characterization. Also, this Chapter includes theoretical background and the important topics related to the problem.

- In Chapter 3 the main experimental setup is presented
- Chapter 4 presents the relationship between the mechanical and acoustical parameters
- In Chapter 5 the results of the evaluation of the methodology applied are discussed.
- Chapter 6 presents the conclusions, contributions and future work of this investigation.

Chapter 2

Framework

2.1 Literature Review

Acoustic characterization has been successfully applied in many fields such as in Medicine. In the audio context, audio signal processing contributed to the development of better medical devices and therapies [8]. However, to our knowledge our application has not been applied to the task of road friction characterization, even though engineers and scientists have been trying to come up with a system that can aid drivers in detecting where roads are likely to be the most dangerous. [21]

Related works can be found in IEEE team work; they decided to see if it would be possible to detect how slippery a road was by analyzing audio feedback from the car tires, and with that purpose they used recurrent neural networks (RNN) - a powerful and robust type of artificial neural network with an internal memory - and a shotgun microphone to monitor all the sounds the rear tire produced when it came into contact with a road during different weather and at varying speeds. [22]

Other examples are found in the video processing domain, where researchers from the University of Toyama in Japan showed off a wetness detection system studied with two camera setups: a surveillance camera at night and a camera onboard a vehicle. The detection of road surface wetness using surveillance camera images at night is relying on passing cars headlights as a lighting source that creates a reflection artifact on the road area [23]. A recent study uses near infrared (NIR) camera to classify several road conditions per every pixel with high accuracy, the evaluation has been made in laboratory conditions, and field experiments [25]. Nevertheless, a drawback of video processing methods is that they require an external illumination source and clear visibility conditions, since results under fog, snow, and poor light conditions show to be inaccurate.

Another approach capable of detecting road wetness relies on 24-GHz automotive radar technology for detecting low-friction spots [26]. It analyzes backscattering properties of wet, dry, and icy asphalt in laboratory and field experiments.

Audio analysis of the road-tire interaction has been done commonly by examining tire noises of passing vehicles from a stationary microphone positioned on the side of the road. This kind of analysis reveals that tire speed, vertical tire load, inflation pressure and driving torque are

primary contributors to tire sound in dry road conditions [27]. Acoustic-based vehicle detection methods, as the one that uses bi-spectral entropy have been applied in the ground surveillance systems [28]. Other on-road audio collecting devices for surface analysis can be found in specialized vehicles for pavement quality evaluation (e.g., VOTERS [29]) and for vehicles instrumented for studying driver behavior in the context of automation (e.g., MIT RIDER [30]).

Finally, road wetness has been studied from on-board audio of tire-surface interaction, where a similar study by the Technical University of Madrid used support vector machines (SVM) – a type of machine learning model – to analyze the sounds from the tire meeting the road and classify the different sounds made by the asphalt. However, the researchers found the range of surface types that could be predicted were limited, and unrelated audio input like the sound of pebbles bouncing against the tires could create false predictions. [2].

The method described on the thesis improves the prediction accuracy of the method presented in [24] and expands the evaluation to a wider range of surface types and pavement conditions. Additionally, the present study is the first one in applying acoustic signals in this field to characterize road friction. For this purpose, the system was tested on different routes and considered all predictions regardless of the speed, pebbles impact or any other factor.

2.2 Theoretical Background

The surface characteristics of the pavements influence various aspects of the operation of a road, such as safety, comfort, travel times, operating costs and dynamics of the vehicles that circulate. Its duration depends on the quality of construction of the pavement, materials used, the wear produced by the vehicles, as well as the deterioration produced by climatic factors, among others. [19]

In Mexico most of the paved roads constitute the so-called "flexible pavements", although there are also sections on motorways and the federal network of roads made up of "rigid pavements". The surface characteristics of both types of pavements must meet certain characteristics that minimize the causes of accidents.

The tires of the vehicles rest on the pavement producing a footprint of different form for each type of vehicle, inflation pressure, load per wheel, speed and surface condition. When the vehicle is immobile or under a small uniform movement there are vertical pressures on the pavement, while when it is in motion there are also horizontal stresses due to friction and trajectory changes. Suctions in the water contained in the pavement and vertical impact forces by effects of vehicle movement and irregularities of the tread surface.

To study the effects that the pavements cause in the circulation it is necessary to appeal to ranges of the geometry of the tread surface. Because of several studies, the International Permanent Association of Highway Congresses has adopted a classification of the different characteristics of the road surface according to the different geometric scales, and its presence

in vehicle-road operation has been identified.

In this way it has been found that the microstructure that has a pavement influences the risk of accidents due to skidding at any speed, as well as the wear of the tires of the vehicles that circulate on the tread surface. [19]

The macrostructure is the relief of the tread layer with the naked eye and is directly related to the surface drainage of the pavement, it influences the water projection of the vehicles during and after a precipitation. Megatexture and surface roughness have an influence on comfort, handling stability, dynamic loads, wear and vehicle operating costs. The surface condition of a road is vital to the overall efficiency of transport.

The adhesion between the tire and the pavement is assessed by measuring the coefficient of friction of the wheel in the presence of water. Traditionally it has been characterized by the friction pendulum, which gives an indirect indication of the degree of roughness of the microstructure of the tread surface. Currently there are several high-performance equipment that, with different principles (trajectory of the wheel, braking wheel, smooth tire, etc.), measure the resistance to friction. On the other hand, texture is a characteristic that is considered more and more important for the good quality of the tread layers, their drainage, their sonority, etc.

The measurement of roughness serves as a parameter of quality control in new roads, reaching to offer economic stimuli when values higher than those specified in the work contract are reached, or sanction otherwise. Surface roughness is currently assessed by a widely diffused indicator called the International Index of Roughness (IRI). For its measurement various equipment are used, mechanical, traditional or other more modern.

In addition to the IRI, there is a parameter called the International Friction Index (IFI), which allows to refer to a standard scale, the texture and friction conditions of a pavement, measured with any type of equipment or method. [19]

2.3 Types of pavements in Mexico

In Mexico, almost all the paved roads are called "flexible pavements". There are also some stretches on concessioned highways and in the federal network conformed with "rigid pavements", with a length of the order of 700 km.

2.3.1 Flexible pavements

Flexible pavements, as shown in Figure 2, are formed by a series of layers (structural section) constituted by materials with decreasing strength and deformability with depth, analogous to the decrease in pressures transmitted from the surface. The asphalt layer is the upper part of the pavement, directly supports traffic requests and provides the functional characteristics of the

road. Structurally, it absorbs the horizontal stresses and part of the vertical efforts.

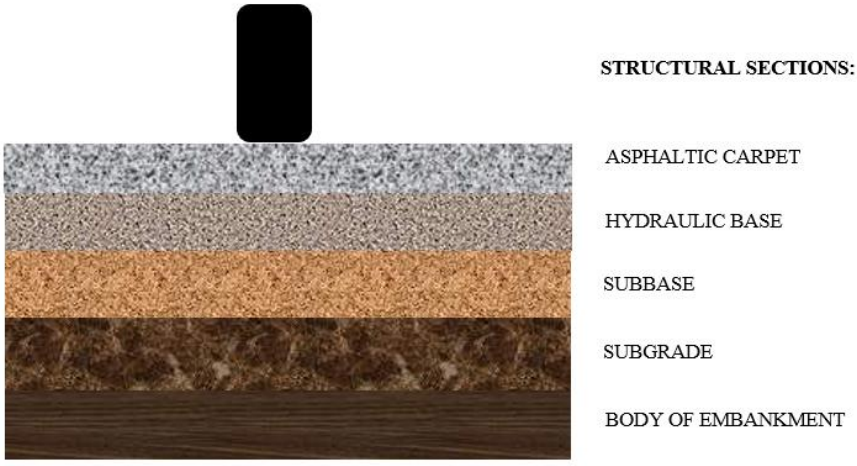

Figure 2 - Typical conformation of a flexible pavement.

Due to the viscoelastoplastic behavior of the asphalt mixtures, the passage of the load, especially under conditions of high temperatures or low speeds, produces an accumulation of plastic deformations.

2.3.2 Rigid pavements

In the rigid pavements, as seen in Figure 3, the slabs of hydraulic concrete constitute the layer of greater structural and functional responsibility; the lower layers of the pavement have the mission to ensure a uniform and stable support for the slab.

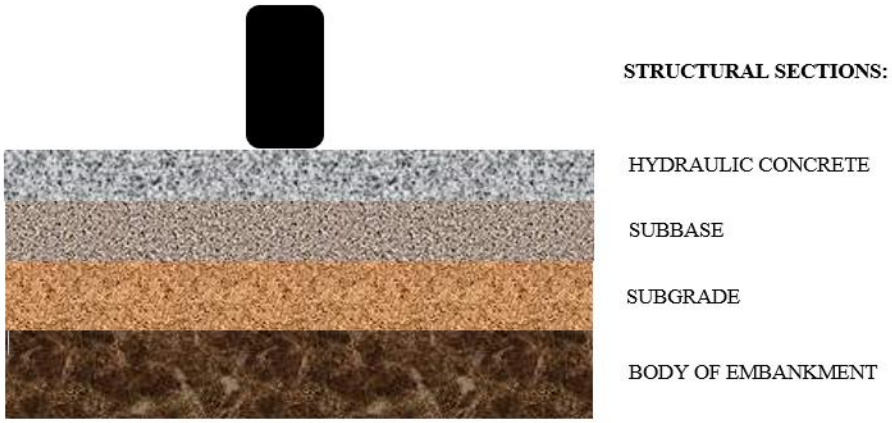

Figure 3 - Typical conformation of a rigid pavement.

The rigidity of the hydraulic concrete layer means that the pavement is resistant to high contact pressures of heavy vehicles. Therefore, these pavements cannot suffer viscoelastoplastic rolling, even in severe conditions of heavy traffic, intense or with high temperatures.

On the other hand, the vertical stresses caused by the loads are widely distributed in the support base of the slab, so that the maximum stress transmitted is only a small fraction of the maximum contact pressure.

Slip resistance is achieved by using a layer of silica sand and giving the fresh concrete a suitable surface texture, by dragging a burlap and by brushing, grooving, etc. The macrostructure must be rough for high circulation speeds and may be smoother for moderate or low speeds. The type of texture also influences the noise produced in the tread, perceived both inside and outside the vehicles.

Hydraulic concrete increases its resistance over time and if the design of the pavement has been correct, its service index decreases more slowly than that of pavements with asphalt layers. [19]

2.4 Tire-Road Interaction

Statistically there is a significant effect of skid resistance on the wet accident rate. The wet accident rate increases with decreasing skid resistance. Skid resistance is described as the resistance a pavement can offer to a braking car under wet conditions. The main characteristic of a road surface that influences skid resistance is its texture. Wet skid resistance decreases with increasing speed and the levels of skid resistance achieved are governed by the interaction between the various components of texture and the tire tread. [9]

Clearly, properties of road surfaces that improve tire/road friction will generally have a positive influence on skid resistance. Properties of tires, however, will influence friction for vehicles using those tires but not skid resistance (apart, from the specialized case of test tires on skid resistance of measurement devices).

When wet conditions are presumed adhesive forces between the road surface and the car tire can be neglected, i.e. adhesion would not contribute a considerable share to the amount of friction generated [10]. Under these friction conditions can totally be allocated to hysteretic effects within the rubber generated by the asperities of the road surface intruding into the tire tread.

Although there are other components of pavement friction (e.g., tire rubber shear), they are insignificant when compared to the adhesion and hysteresis force components. Thus, friction can be viewed as the sum of the adhesion and hysteresis frictional forces [11], as seen in Equation (1). A schematic representation of the phenomena is also shown in Figure 4.

$$F = F_A + F_H \tag{1}$$

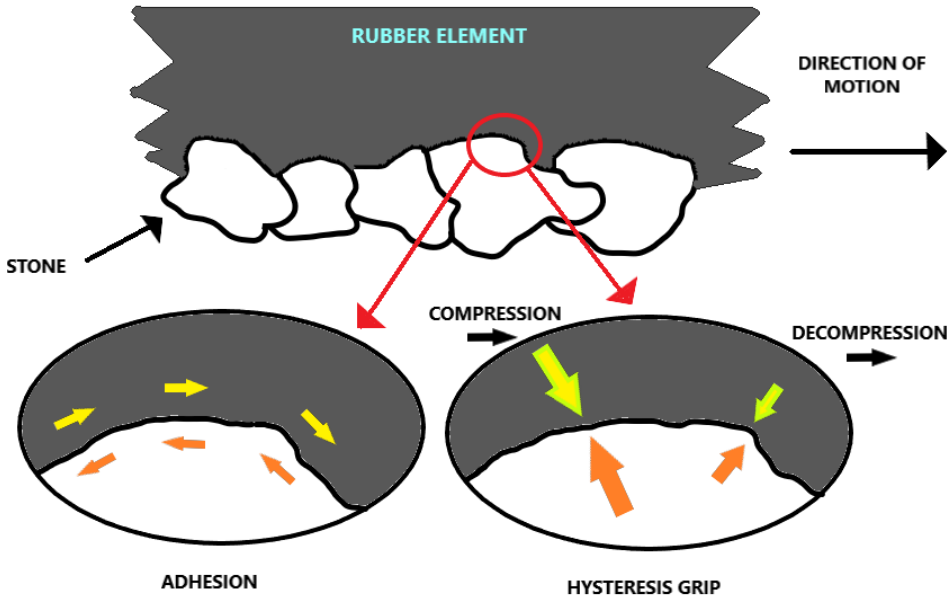

Figure 4 - Schematic Plot of Hysteresis and Adhesion

2.4.1 Factors Affecting Pavement Friction

Numerous factors can influence the magnitude of the frictional force generated between the tire and pavement surface, and Table 1 presents the most important. Friction must be viewed as a process instead of an inherent property of the pavement. It is only when all these factors are fully specified that friction takes on a definite value.

Table 1 – Factors affecting pavement friction. Modified from [53]

Pavement Surface Characteristics	Vehicle Operating Parameters	Tire properties	Environment
-Microtexture		**-Tread design and condition**	**-Temperature**
-Macrotexture	**Slip speed:** **-Vehicle Speed** **-Braking action**	**-Inflation pressure**	**-Water (rainfall, condensation)**
-Material properties		-Foot print	**-Snow and Ice**
-Megatexture/ unevenness	Driving maneuver: -Turning -Overtaking	-Rubber composition	**-Contaminants: Salt, sand, dirt, mud, debris**
-Temperature		-Load -Temperature	-Wind

***Critical factors are shown in bold**

The surface must provide enough macro-texture to assist effective drainage of water from the road/tire interface and increase the zone of potential dry contact at the rear of the tire/road contact patch. However, drainage alone is not enough to provide good skid resistance; the water film can only be broken if the road surface has a good micro-texture on which localized high pressures are built up [12].

Some researchers have indicated that micro-texture is the single most important factor at both low and high speeds in providing adequate friction at the tire pavement interface [13].

Otherwise, the PIARC experiment strongly confirmed that macro-texture is recognized as a major contributor to friction safety characteristics for several reasons. The most well-known reason is the hydraulic drainage capability that macro-texture has for wet pavements during or immediately after a rainfall. This capability will also minimize the risk for hydroplaning. Another reason is that the wear or polishing of macro-texture can be interpreted as it changes its value over time for a section of road [11].

2.4.2 Pavement Surface Characteristics

To analyze the effects that the pavements (flexible and rigid) cause in vehicles, it is necessary to use small scales that allow to appreciate magnitudes of the order of tenths of a millimeter or even smaller. The A.I.P.C.P. proposed a classification of surface geometrical characteristics based on wavelengths and amplitudes of irregularities, as shown in Table 2.

Table 2 - Classification of surface irregularities of a pavement (flexible or rigid).

NAME		RANGE OF DIMENSIONS (APROX.)	
		HORIZONTAL	VERTICAL
*MICROTEXTURE		0 - 0.5 mm	0 - 0.2 mm
*MACROTEXTURE		0.5 - 50 mm	0.2 - 10 mm
*MEGATEXTURE		50 - 500 mm	1 - 50 mm
*SUPERFICIAL REGULARITY	Short waves	0.5 - 5 m	1 - 20 mm
	Medium waves	5 - 15 m	5 - 50 mm
	Long waves	15- 50 m	10 - 200 mm

The vehicle-road interaction causes these surface irregularities to influence to a greater or lesser degree, depending on their wavelength. Figure 5 shows the range of irregularities of flexible and rigid pavements that affect the user; however, some of them are necessary for the safety of vehicles. [19]

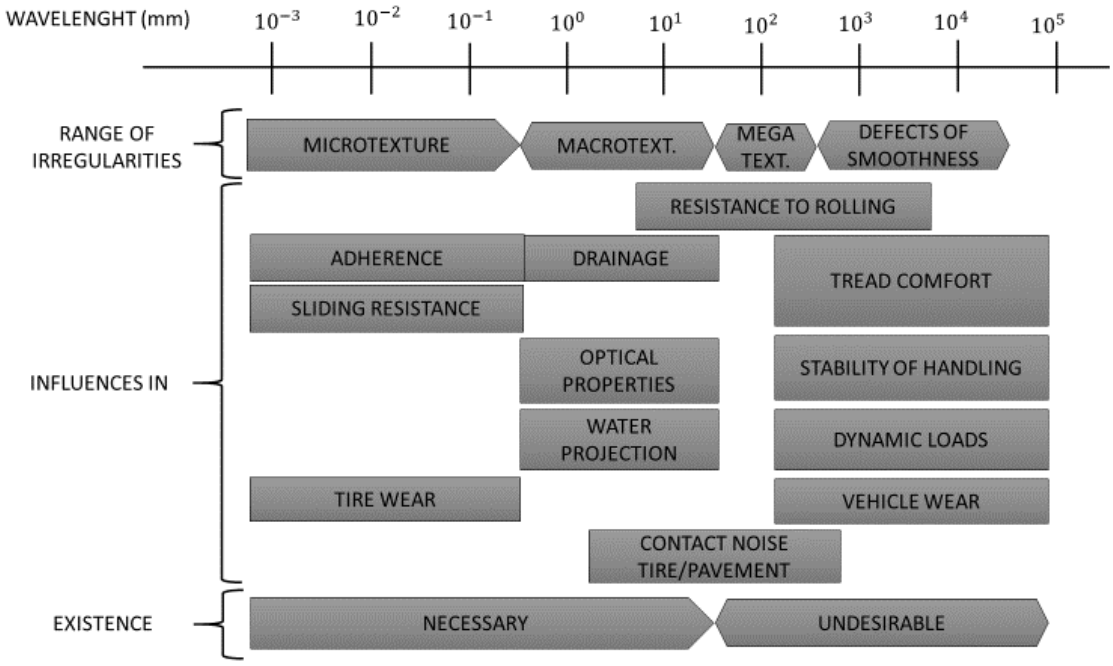

Figure 5 - Influence of the range of surface irregularities in the phenomena of interaction between vehicles and the road. [12]

Chapter 3

System Design

3.1 Mechanical characterization of pavement surface

3.1.1 Differentiation of equipment

The following diagram in Figure 6 shows a schematic representation of some of the equipment used nowadays for pavements surface measurement and characterization divided by application and mobility.

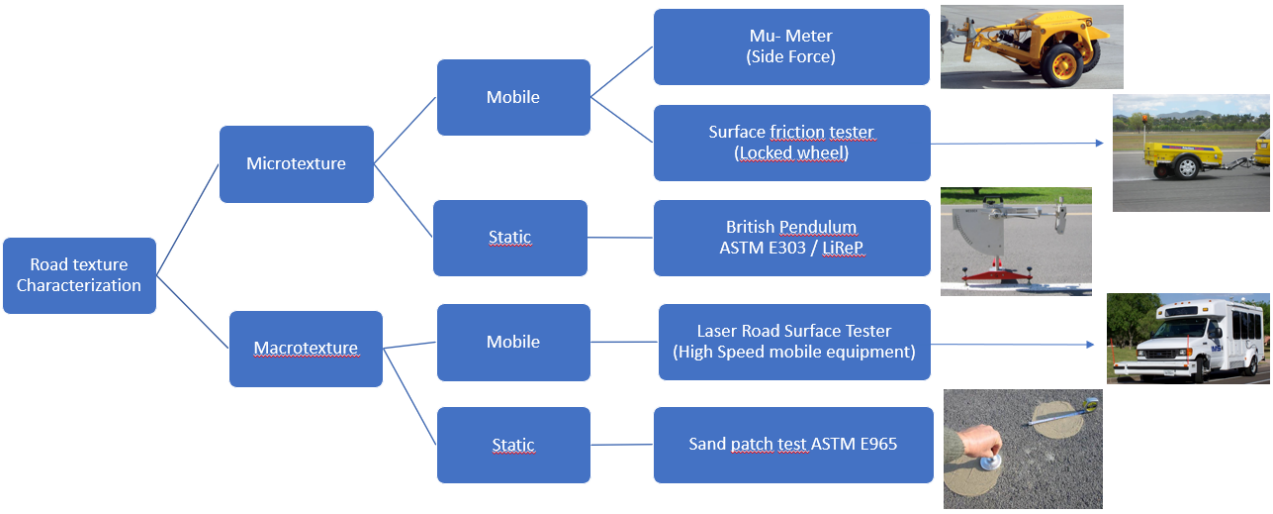

Figure 6 – Example of equipment used to characterize asphalt

For our experimentation we had access to the British pendulum and the sand patch test.

3.1.2 British Pendulum Test (Microtexture)

Description

The purpose of the procedure is to obtain a Slip Resistance Coefficient (S.R.C.) which, maintaining a correlation with the physical coefficient of friction, evaluates the anti-slip characteristics of a pavement surface. The results obtained by this test are not necessarily

proportional or correlative with friction measurements made with other equipment or procedures.

This test, as seen in Figure 7, consists in the loss of energy measurement through a pendulum of known characteristics provided at its end of rubber. The edge rubs with a certain pressure on the surface to be tested and on a fixed length. This energy loss is measured by the supplementary angle of the pendulum oscillation.

The test method can also be used for measurements on industrial buildings pavements, laboratory tests on specimens, tiles or any type of sample of finished flat surfaces. [15]

For further information about the experimental procedure to prepare the equipment, please refer to Appendix A.

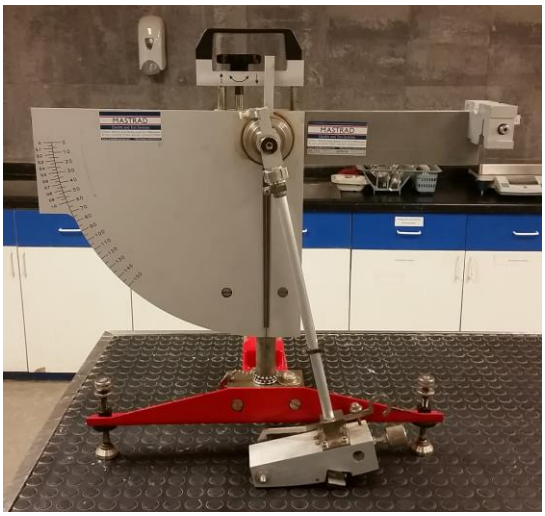

Figure 7 - British friction pendulum (ASTM E 274)

Calculation

Although the British pendulum tester is not a new device, further discussion to review certain important aspects of the tester performance would be beneficial.

The basic concepts of design and operation of the British pendulum tester were described by Giles et al. and by Kummer and Moore [16]. Figure 8 shows a schematic of the tester. The differential equation of motion derived from the energy conservation is the following mathematical expression:

$$I\ddot{\theta} + WLsin\theta = FL(sin\theta + \mu cos\theta) \quad (2)$$

Where:

θ = angular displacement of the pendulum arm from vertical position,
I = moment of inertia at the center of rotation,
W = weight of the arm,
L = distance from the center of rotation to the slider,
F = normal force applied by the rubber slider to the test surface, and
μ = coefficient of friction of the test surface.

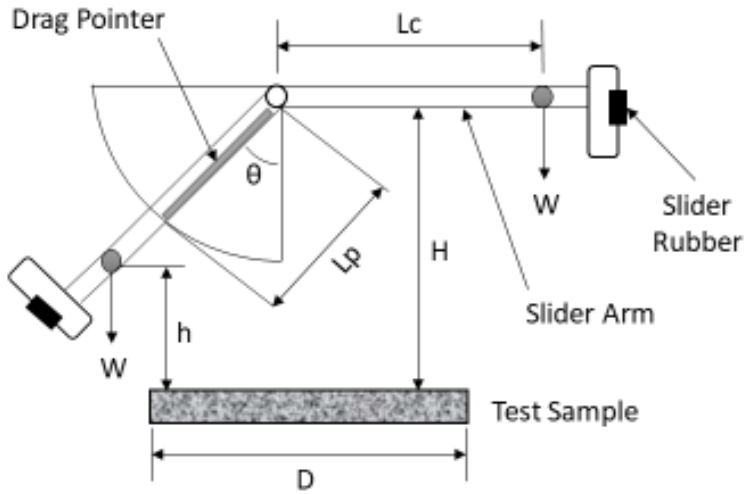

Figure 8 – Schematic of British Pendulum tester

The variable that is most important for the performance of the British pendulum tester is the normal force, F, applied by the rubber slider as it is propelled over the teste surface. The sensitivity of the British pendulum tester to the slider normal force can be calculates as:

$$S_{FN} = \frac{\Delta BPN}{\Delta F_N} = 1.83 \frac{BPN}{N} \tag{3}$$

The slide resistance coefficient of the British pendulum is obtained as following:

$$S.R.C. = \frac{Effective\ reading\ (FRs)}{100} \tag{4}$$

The measurements made on the pavement are always affected by the temperature variations of the rubber and the surface tested; therefore, to the value obtained from the pendulum is added a factor to the effective reading. Further information about the temperature correlation factor can be found in Appendix A.

For road quality purposes, the Mexican government suggested Table 3 for friction values measured with the British pendulum in wet pavement (critical condition):

Table 3 - Microtexture values proposed by the Mexican government. [17]

Friction (S.R.C.)	Assessment
< 0.32	Prohibited
0.32 - 0.42	Bad
0.42 - 0.52	Good
> 0.52	Very good

3.1.3 Sand Patch Test (Macrotexture)

Description

This test method is suitable for field tests which determines the average thickness of the macrotexture of the surface of the pavement. The knowledge of the thickness of the macrotexture serves as a tool in the characterization of the surface textures of pavements.

When used in conjunction with other physical tests, the thickness of the macrotexture derived from this test method can be used to determine the sliding resistance capacity of the materials in pavements or the suggestion of a better finish. When used with other tests, care must be taken that all of them apply to the same place.

The measurements of the thickness of the texture produced using this method of the test is influenced by the characteristics of the macrotexture of the surface. The particle shape of the aggregate, size and distribution are characteristics of the surface texture not considered in this procedure. This test method does not attempt to provide a complete qualification of surface texture characteristics.

The values of the thickness of the surface macrotexture in the pavement determined by this method, with the material and procedures established here, do not necessarily agree or correlate directly with other surface texture measurement techniques.

The surface of the pavement to be sampled using this test method should be dry and free of any construction debris, surface debris, and loose aggregate particles that could be removed or displaced during normal environmental and service conditions. [18]

Experimental Procedure

The materials and standard test method consist of a uniform amount of material, a container of known volume, a screen suitable for protection against the wind, brushes to clean the surface, a flat disk to disperse the material on the surface and a ruler or any other device to determine the

area covered by the material, all of these shown in Figure 9. A weighing scale is also recommended to ensure the consistency of the measurements of each assay. Further information about more test procedure details and its required equipment please refer to Appendix A.

Figure 9 – Sand patch test (ASTM E 965)

Calculation

Cylinder volume. - Calculate the internal volume of the test cylinder as follows:

$$V = \frac{\pi * \phi^2 * H}{4} \quad (5)$$

Where:

V = internal volume of the cylinder, in3 (mm3),

ϕ = diameter of the test cylinder, in (mm), and

H = cylinder height, in (mm).

Average thickness of the macrotexture of the pavement. - Calculate the average of the macrotexture of the surface using the following equation:

$$H = \frac{4 * V}{\pi * \phi^2} \quad (6)$$

Where:

H = average thickness of the macrotexture of the surface, in (mm),

V = volume of the sample, in3 (mm3), and

ϕ = average diameter of the area covered by the material in, (mm).

For road quality purposes, the Mexican government suggested Table 4 for macrotexture values measured with the Sand patch test in dry pavement:

Table 4 - Macrotexture values proposed by the Mexican government. [17]

Texture (mm)	Assessment
< 0.43	Prohibited
0.43 - 0.63	Bad
0.63 - 0.83	Good
> 0.83	Very good

3.1.4 International Friction Index

Description

This section presents a description to obtain the International Friction Index (IFI) from texture and slip resistance measurements, and finally, its interpretation and application to evaluate the surface conditions of the pavement, in the interest of road safety.

The sliding resistance capacity was evaluated in two different ways:

- Directly measuring the coefficient of friction between the tire and the wet pavement
- Analyzing the macrotexture or the surface drainage capacity of the pavement (to estimate the reduction in adherence that occurs when increasing speed).

The procedure is presented to determinate the IFI using the British Tester and the Sand Patch Test in road sections with several surface conditions.

An example to calculate the values of the IFI is presented step by step. Showing tables of field data and later the processing of said data, until reaching the IFI value characteristic of the section.

The PIARC model can be used in the administration of pavements establishing levels of intervention of the IFI, considering certain values or minimum levels of friction and texture, according to the prevailing conditions and the needs required in each type of road. To do this, a diagram was created to indicate the relationship between the friction values, FRs, and the texture values, TX, as shown later on this document.

In conclusion, the main advantage is the obtainment of a common scale of friction values called IFI in which all the results of friction measurements in road pavements and airports are

included with an acceptable precision. Final discussions are made about its interpretation and implementation to generate a relationship between the results measured and our acoustical system. [52].

Calculation

The PIARC model is the basis of the definition of the International Friction Index, IFI, through the parameters F60 and Sp. Thus, the IFI of a pavement is expressed by the pair of values (F60, Sp) expressed in parentheses and separated by a comma; the first value represents the friction and the second the macrotexture.

The first is a dimensionless number and the second is a positive number with no limits and with units of speed (km/h). The friction zero value indicates perfect slip and the value one, grip. It is not possible, for the moment, to describe with a simple relation the second number that makes up the IFI.

During the elaboration of the model, and from the data of the PIARC experiment, it has been verified that the velocity constant Sp can be determined by means of a linear regression in function of the field measurement of the macrotexture (TX) such that:

$$\mathrm{Sp} = \mathrm{a} + (\mathrm{b} * \mathrm{TX}) \tag{7}$$

Where the values of the constants “a” and “b” for the Sand Patch Test equipment (ASTM E965) are:

$$\mathrm{a} = -11.6\,, \mathrm{b} = 113.6$$

The value of the FR60 constant is determined using the friction value FRs obtained in the field with some equipment at the slip speed S, where we obtain:

$$\mathrm{FR60} = \mathrm{FRs} * e^{\frac{s-60}{Sp}} \tag{8}$$

Finally, the desired value of F60 is obtained through the following correlation with FR60 established by the PIARC experiment:

$$\mathrm{F60} = \mathrm{A} + (\mathrm{B} * \mathrm{FR60}) \tag{9}$$

Where A and B are constants according to the equipment used to measure Friction, and their values for the British Pendulum Tester are:

$$\mathrm{s} = 10\ \mathrm{km/hr}, \mathrm{A} = 0.056, \mathrm{B} = 0.008$$

The knowledge of these parameters also allows knowing the estimated reference curve of friction as a function of the sliding speed according to the following equation:

$$F(s) = F60 * e^{\frac{60-s}{Sp}} \quad (10)$$

The representative Sp and F60 values are replaced for each section given. Once these parameters have been calculated, and using Equation (10), the estimated friction values F for the velocity of time are calculated.

Acceptance/Rejection Graph

The PIARC model can be used in the administration of pavements establishing levels of intervention of the IFI, considering certain values or minimum levels of friction and texture, according to the prevailing conditions and the needs required in each type of road.

To do this, a diagram is used that relates the texture values (TX) with the friction values (FRs) in the axes, and this applies to any equipment used to measure these parameters. In the diagram is located the curve that will define the border of minimum permissible values, friction (F curve) and the T Line related to the recommended minimum value of texture. [20].

Figure 10 shows how each area of the graph should be interpreted, and thus be able to consider whether the section under study has the proper characteristics of friction and texture. This graph can be used for two purposes:

- The first case as support to know what kind of texture will give us the speed of operation, such that for critical conditions (wet pavement), the vehicles operate safely.
- The second, as a road adviser, establishing whether to improve the micro- or macrotexture.

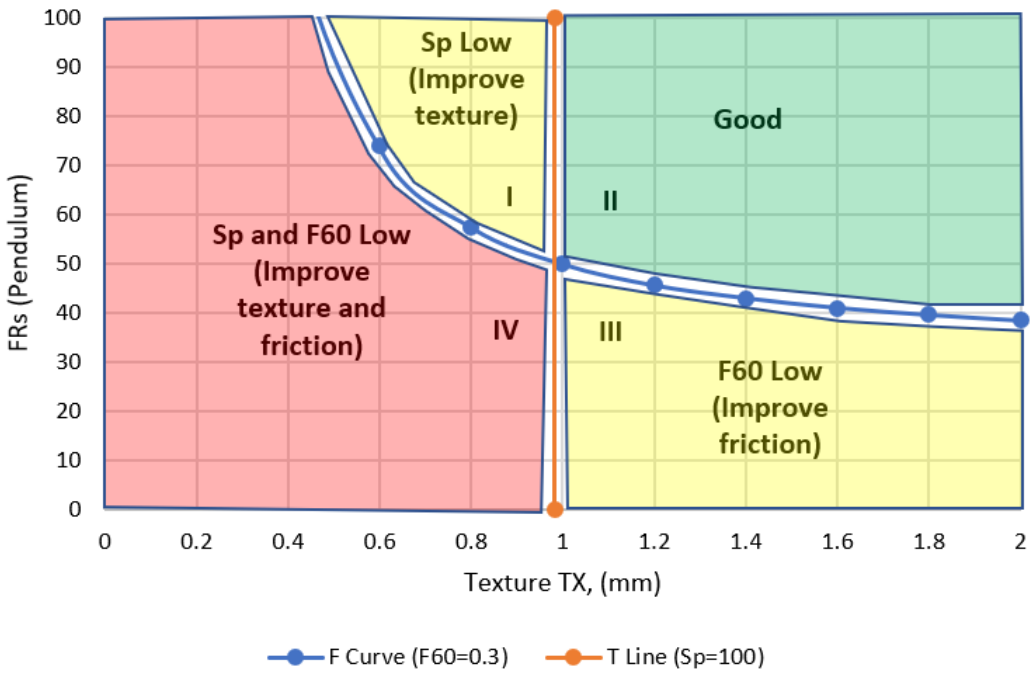

Figure 10 - Interpretation areas of the diagram Friction vs. Macrotexture [15]

The interpretation of each of the quadrants in Figure 10 is as follows:

I. In the first quadrant we find that the pavement surface requires improving the macro texture, this may be possible by improving with the placement of a seal irrigation or a micro folder with the appropriate design that allows to dislodge the volume of water that is present by the specific precipitation from that place.

II. In the second quadrant, (following clockwise) according to our limits of F60 and Sp, we will find the points that fulfill with an adequate micro- and macro texture for the needs of our road.

III. In the third quadrant, we found that it is necessary to improve the micro texture, that this could be if the quality of the stone material of the folder is improved (or if hydraulic concrete is used, taking care that it has a good scratch).

IV. In the fourth quadrant, the most critical situation of the pavement is presented, since it is necessary to improve both, micro- and macro texture.

3.2 Acoustic parameters of road surface

3.2.1 Modeling of random ground roughness effect by an effective impedance

Natural grounds can exhibit small scale geometric irregularities, compared to the acoustic

wavelength, known as ground roughness. Ground roughness has noticeable effects on outdoor sound propagation, since it shifts the ground dip due to the ground effect towards the lower frequencies and it leads to the formation of a surface wave.

In the context of prediction methods improvement for outdoor sound propagation, using an effective impedance appears to be a useful approach to model the effects of surface roughness. The boss model approach allows to express an effective impedance Zeff (or an effective admittance βeff= 1/Zeff) for a ground roughness formed by regular scatterers, such as semi-cylinders [36], as shown in Figure 11.

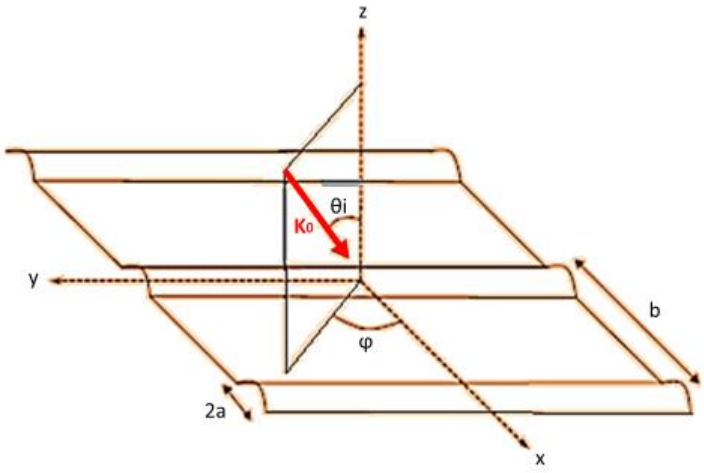

Figure 11 - Wave vector **K0** incident to a surface containing cylinders of radius a and mean center-to-center spacing b [37].

The effects of roughness are considered as a correction to the surface admittance βS, and Zeff is given by:

$$\frac{1}{Zeff} = \beta\text{eff} = \beta\text{s} + \beta\text{R} \tag{11}$$

Where βs is surface admittance ($\frac{1}{Zs}$), Zs is base impedance, and the correction βR is function of the angles θi and φ, the frequency, and other parameters depending of the scatterers' size, shape and spacing.

An effective impedance model for random roughness was developed in [36]. Using the Small Perturbation Method (SPM), it models the mean effects of random ground roughness characterized by a roughness spectrum, such as the Gaussian roughness spectrum which is defined by two statistical parameters. Just like the boss model formulation, for an absorbing ground, the ground roughness effect is modeled as a correction to the base admittance of the ground surface.

In the SPM model for random roughness a 2D rough surface showing a small and slowly-varying roughness is considered, as shown in Figure 12. In this figure K0 and its modulus are

respectively the wave vector and the wave number in the air, with C0 the sound speed in the air, ξ(x) is the height profile, θi is the angle of incidence, Z0 is the characteristic impedance of the air and Zs is the impedance of the surface.

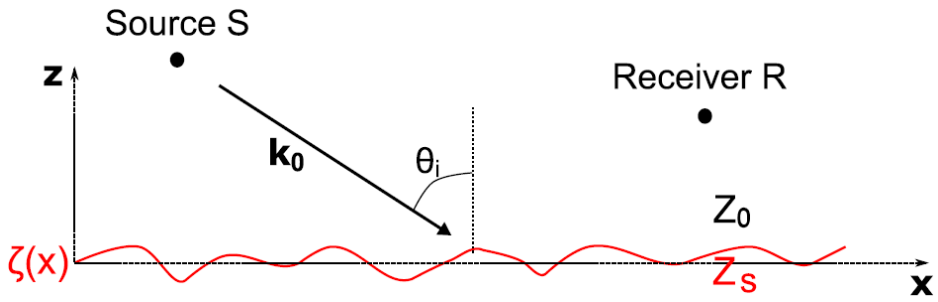

Figure 12 - Wave vector **K0** incident to a rough surface ξ

Two dimensional TLM simulations of 50m propagation above absorbing and rigid random rough grounds (whose roughness was defined by a Gaussian spectrum) were performed in [36], and the results were compared to analytical solutions calculated with the SPM effective impedance model, which showed that the SPM effective impedance accurately takes into account the mean effects of roughness on sound level spectra, and also correctly models the roughness induced surface wave.

SPM effective impedances were implemented in FDTD and TLM codes by approximating the effective impedance by a sum of rational functions, using the vector fitting technique to identify the coefficients of these functions. FDTD and TLM numerical methods with SPM effective impedance have been proven to be efficient and useful for simulating complex middle-range propagation cases with time-domain methods, as they allow to consider quite easily the mean effects of a statistically defined roughness. [36]

It should be pointed out that in order to be used in time domain, an impedance model must be physically admissible and verify reality, causality and passivity conditions [38,39]. The Miki model with thickness effect was the base impedance model considered to derive the SPM effective impedance for the considered grounds using (47). Recent studies [40,41] showed that the Miki model is actually not physically admissible, and not the best suited model for long-range outdoor sound propagation predictions despite its common use. Furthermore, this SPM effective impedance approach should still prove functional using more refined base impedance models, such as the slit pore model [42].

A promising application for effective impedance models and particularly for the SPM model would be to use them in engineering methods for an acoustic characterization of road pavements. This would require experimental data to characterize roughness spectra of pavements.

3.2.2 Theoretical model of acoustic system proposal

An outline of this configuration is presented in Figure 13, which is considered a primary point source situated at a height *Zs* and a receiver located at a height *Zr* above the ground surface. This porous surface is treatment as a flat surface, consisting of a semi-infinite field, an absorbing layer on a rigid layer or a combination of different absorbent layers. In all cases, the surface is homogeneous, and the propagation is in the atmosphere.

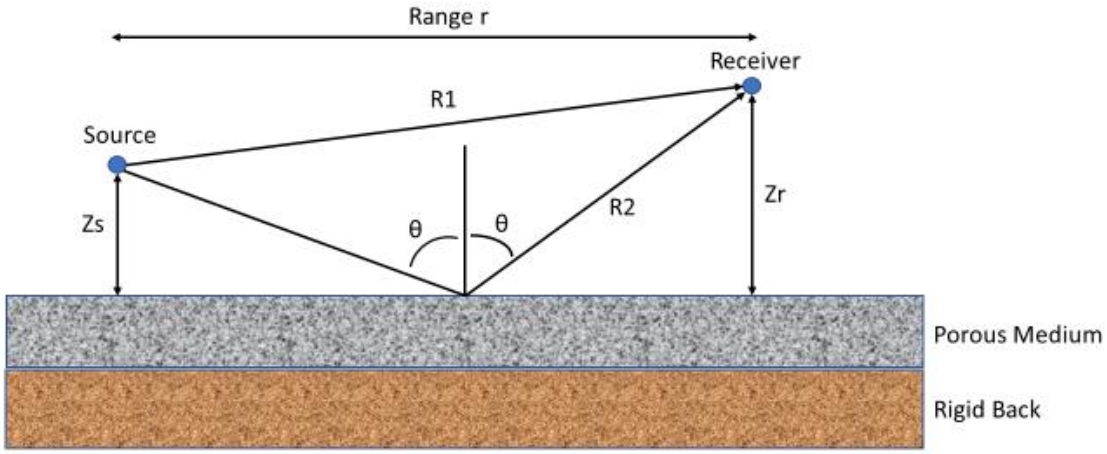

Figure 13 - Geometry to study the attenuation between source and receiver in presence of a porous ground formed with several absorbent layers

The sound pressure at the receiver is the sum of the direct signal, which comes from the real source, plus the reflected signal from the ground, which is assumed to come from the image source.

The method consists on measuring the sound level difference from two microphones close to the surface and calculating the level difference according to an impedance model of the ground.

To solve this problem, it is assumed that the total potential is because a direct contribution from the source to the receiver, and a contribution of the reflected part in porous surface, of the form [31].

$$\phi = \frac{e^{ikR_1}}{4\pi R_1} + Q_1 \frac{e^{ik2R_2}}{4\pi R_2}, \tag{12}$$

where Q_1 is the reflection coefficient of the spherical wave for the point source on the outer surface with a finite impedance, R_1 is the distance between the point source and the receiver and R_2 is the traveled path by the reflected wave between source and receiver, as shown in Figure 13. Knowing the angle of incidence of the reflected wave and the specific admittance β, which defines the properties of the absorbing surface, the reflection coefficient of the spherical wave can be calculated with the expression:

$$Q_1 = R_p + \left(1 - R_p\right) F(w_1) \tag{13}$$

where:

$$R_p = \frac{cos\theta - \beta}{cos\theta + \beta} \tag{14}$$

is the reflection coefficient of the plane wave, and the function $F(w_1)$ is called the boundary loss factor, given by the expression:

$$F(w_1) = 1 + i\sqrt{\pi} w_1 e^{-w_1^2} erfc(-iw_1) \tag{15}$$

where *erfc ()* is the complementary error function, and w_1 is the numerical distance that is calculated as:

$$w_1 = \sqrt{\frac{1}{2} ikR_2}(cos\theta + \beta) \tag{16}$$

To use these equations, a model for the specific impedance of the absorbing surface was needed. Preliminary, in this work three different situations have been considered. The simplest case is a semi-infinite homogeneous medium that fills the bottom space bounded by the surface. Then, the specific admittance has the expression:

$$\beta = m_1 \sqrt{n_1^2 - sin^2\theta} \tag{17}$$

were:

$$n_1 = \frac{k_1}{k}, \quad \text{and} \quad m_1 = \frac{\rho}{\rho_1} \tag{18-19}$$

In Equations (18-19) k_1 is the complex wave number of propagations in porous medium and ρ_1 the density of the porous medium.

If the absorbing surface is comprised of a layer of porous material above a rigid surface, the admittance specific expression is:

$$\beta = -jm_1 \sqrt{n_1^2 - sin^2\theta} \tan\left(kd_1 \sqrt{n_1^2 - sin^2\theta}\right) \tag{20}$$

where *d* is the thickness of the porous layer in contact with the surface.

Finally, if we consider two porous layers, the specific admittance is given by:

$$\beta = -jm_1 \sqrt{n_1^2 - sin^2\theta} \frac{\tan\left(kd_1 \sqrt{n_1^2 - sin^2\theta}\right) + g_1 \tan\left(kd_2 \sqrt{n_2^2 - sin^2\theta}\right)}{1 + g_1 \tan\left(kd_1 \sqrt{n_1^2 - sin^2\theta}\right) \tan\left(kd_2 \sqrt{n_2^2 - sin^2\theta}\right)} \tag{21}$$

where:

$$g_1 = \frac{m_2\sqrt{n_2^2 - sin^2\theta}}{m_1\sqrt{n_1^2 - sin^2\theta}} \tag{22}$$

This dimensionless factor characterizes the change of acoustic propagation properties between the two-porous media. [32,33]

According to this model, the ground attenuation will be:

$$\Delta L = 20\ log_{10}\left[\left|1 + Q\,\frac{R_1}{R_2}\,e^{jk_0(R_2 - R_1)}\right|\right] \tag{23}$$

Thus, a ground impedance model is required to calculate the effect of this boundary in the sound field. Impedance models of one, two, three or four parameters can characterize each of the ground layers.

Let us consider a plane wave incident on a surface with angle $\theta_{0,}$ characterized by acoustic impedance Z_s and propagation constant k_s, as seen in Figure 14.

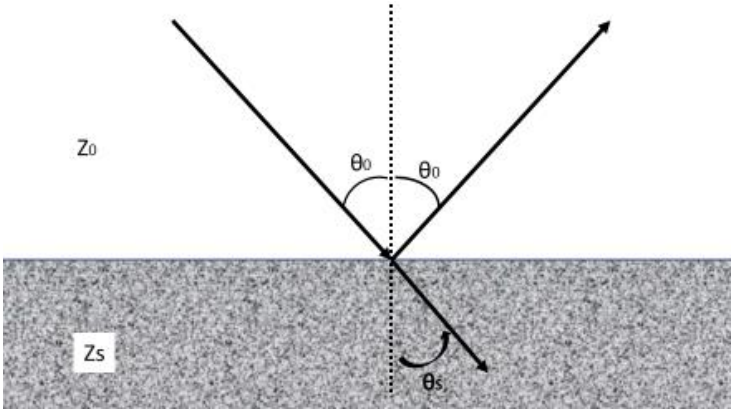

Figure 14 - A plane wave incident on a homogeneous medium.

The impedance model, Z_S, is established for the ground. In this case, a homogeneous locally reacting ground is assumed with normalized acoustic impedance given by the Delany-Bazley equation for one parameter model [34]

$$z_s = (1 + 0.0571E^{-0.754} + j0.087E^{-0.732}) \tag{24}$$

where $E=r_0f/\sigma$, r_0 is the air density, σ is the flow resistivity, and f the frequency.

This model, which depends on just one parameter (the flow resistivity) has been adopted in some works for calculating the excess attenuation of grounds [35].

3.2.3 Experimental methodology based on previous work

The experimental measurements were performed along several pavements, in Mexico City. The following equipment was used: two small acoustic sensors, with frequency response of 20–20,000 Hz; small directional source with frequency response of full range; audio interface of two channels, with sampling frequency of 96 kHz; a laptop and software for signal processing. The two sensors were mounted on a support and a base of wood for the source and were installed in a sports utility vehicle as shown in Figure 15. The sensors were placed at different heights from the soil: 0.06 m and 0.165 m; the source was at a height of 0.165 m, and the distance between sensors and source was 0.45 m. The geometry setup recommended by ANSI S1 standard [43] was slightly modify due to the conditions and the portability.

The purpose of this setup was to measure the sound level difference of two sensors, when the source radiates a MLS (Maximum Length Sequence) signal from a horizontal distance to the sensors. The parameters of a ground impedance model were modified and compared with the experimental curve. The difference in the impedance of the soil between the experimental and the theoretical curves is minimized [44].

The ANSI S1.18 standard covers a frequency range of 250 Hz to 4 kHz. It recommends using a signal with level at least 10 dB above the background noise level. In any case, a cover was used for the sensors. The soil must be flat. The recommendations of the standard were accomplished.

Figure 15 - Experimental setup.

The source can be seen oriented in the direction of the support holding the two sensors. Firstly, a measurement was made in a static position, then at different speeds 10-100 km/h for different pavements along of the city [24]. Figure 16 shows the level difference curves measured at various speeds: 0, 20, 50 and 100 km/h. It shows that, as the speed increases, the resulting curve is not affected by aerodynamic and background noises due to the unwanted reflections and the noise was filtered.

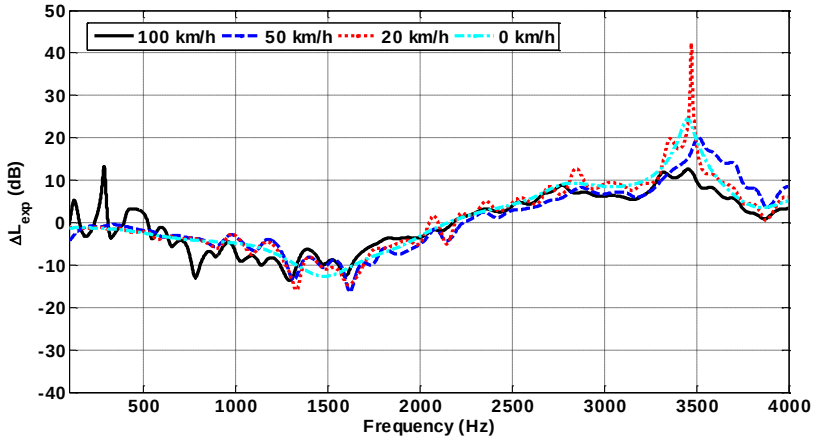

Figure 16- Experimental difference curves at different speeds with noise filtered.

Getting surface parameters

Weather conditions are important, since the determination of sound propagation requires information on temperature, relative humidity and barometric pressure as a function of height near the propagation path. These values determine the sound speed profile. Ideally, the altitude at which the meteorological data are collected should reflect on the application.

In order to make the comparison and adjustment between the experimental and theoretical curves, an algorithm in Matlab was implemented establishing all the ranges for each parameter under test, and a nonlinear programming that attempts to find a constrained minimum of a scalar function of several variables starting at an initial estimate. This is generally referred to as constrained nonlinear optimization [45]. For more information about the Matlab Graphical User Interface (GUI), go to Appendix B.

The frequency fitting range for comparing the theoretical curves, for this case is 1 – 5.5 kHz, due to the absorption and reflection in the path. In Figure 17, the result shows the three parameters and two related parameters (texture and μ), in the case of a speed of 100 km/h: σ = 0.78 x 106 N s/m4, φ = 0.68 and ζ = 0.46; the graphic shows the experimental signal (red) and the theoretical (black) curve, displaying minor discrepancies between them.

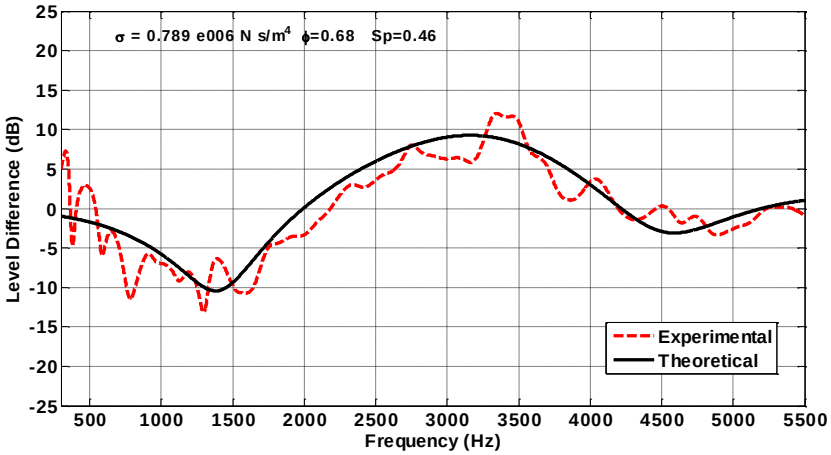

Figure 17- Theoretical and experimental level difference curves for the asphalt at 100 km/h.

Table 5 displays the three parameters obtained at different speeds, acquired along 100 km of some streets and avenues. As can be seen, the three parameters are consistent and reasonable, with the flow resistivity parameter showing more variation, between 0.6 - 1.2 x 106 N s/m4. According with these results, the texture of the pavements can be classified in micro and macro textures likewise the friction coefficient was related and estimated [46].

Table 5 - Surface parameters obtained at different speeds.

Speed (km/h)	Flow Resistivity (N s/m^4 x 10^6)	Porosity	Shape Factor	Texture	Friction Coefficient
0	0.78	0.9	0.5	Macro	> 0.6
10	1.2	0.91	0.52	Macro	> 0.6
20	0.95	0.9	0.51	Macro	> 0.6
30	1.1	0.92	0.52	Macro	> 0.6
40	0.92	0.9	0.5	Macro	> 0.6
50	0.95	0.29	0.4	Micro	< 0.6
60	0.67	0.9	0.51	Macro	> 0.6
70	0.95	0.56	0.45	Micro	< 0.6
80	0.61	0.54	0.44	Micro	< 0.6
90	0.7	0.45	0.42	Micro	< 0.6
100	0.78	0.68	0.46	Macro	> 0.6

Figure 18 shows a comparison between factors at 0 and 100 km/h, from which we conclude that for flow resistivity, porosity and shape factor the value is relatively maintained.

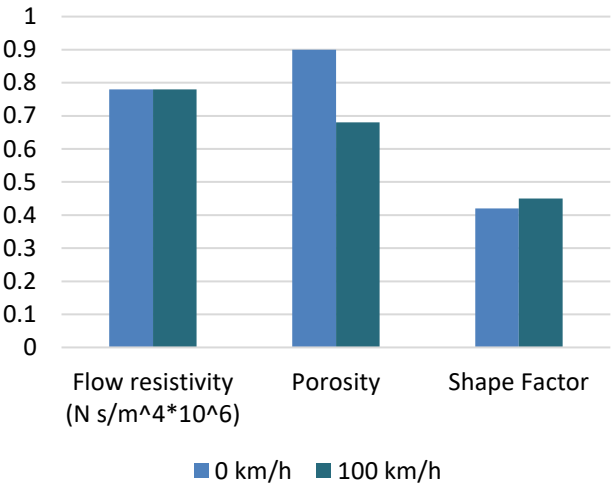

Figure 18 - Comparison chart of flow resistivity, porosity and shape factor at 0 and 100 km/h

Chapter 4

Methods

The main experimental methodology was divided in two parts. The first part consisted in measuring the microtexture (friction) and macrotexture of pavement at 5 different street locations around the ITESM – Campus Monterrey, as seen in Figure 19. Meanwhile, the second part consisted in obtaining the acoustic properties from the same asphalt locations in static and dynamic mode. The British pendulum test was used to measure friction, the sand patch test to measure texture, and an acoustic system was proposed to obtain characteristic properties such as porosity, tortuosity, shape factor and flow resistivity of the pavement. The purpose of this experimentation was to compare results between the different methods and create relationships between the mechanical and acoustical pavement characterization systems.

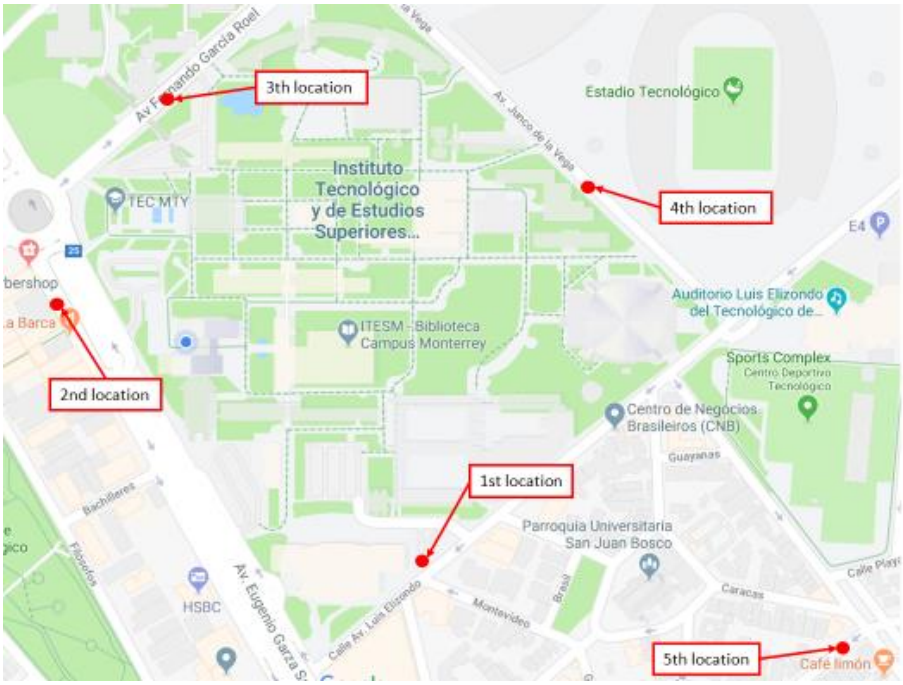

Figure 19– Location of measurements around the ITESM – Campus Monterrey

4.1 Measurements with Mechanical Equipment

4.1.1 Friction measurement with British Pendulum Test

Figure 20 shows an example of a measurement carried out with the British pendulum at Location 1. Furthermore, Table 6 shows the friction values obtained for each of the five points where the measurements were made at a temperature of 14°C.

Figure 20 – Friction measurement at 1st location

Table 6 – Friction values measured with the British pendulum on road surfaces

	1st Location	2nd Location	3th Location	4th Location	5th Location
Average FRs	58	65	54.8	53.4	52
Temperature (°C)	14	13.5	13.5	15.5	15.5
Skid resistance factor	-1.6	-1.7	-1.7	-1.3	-1.3
Friction (S.R.C)	**0.564**	**0.633**	**0.531**	**0.521**	**0.507**

According to the values measured it is concluded that the order of friction (S.R.C.) from better to worse is as following:

1) 2nd location (0.633)
2) 1st location (0.564)
3) 3th location (0.531)
4) 4th location (0.521)
5) 5th location (0.507)

4.1.2 Macrotexture measurement with Sand Patch Test

Figure 21 shows an example of the measurements carried out with the Sand patch test at Location 3. Furthermore, Table 7 displays the macrotexture values obtained for each of the points where the measurements were made.

Figure 21– Macrotexture measurement at 3th location

Table 7 – Sand patch test measurements (mm)

	Diameter of Circle (mm)									
	1st Location		2nd Location		3th Location		4th Location		5th Location	
	T1	T2	T1	T2	T1	T2	T1	T2	T1	T2
ϕ Ave. (mm)	196.25	196.25	188.75	212.5	290	287.5	411.25	435	183.75	186.25
Macrotexture (mm)	**0.942**		**0.911**		**0.435**		**0.203**		**1.060**	

According to the values measured, it is concluded that the order of macrotexture (mm) from better to worse for the five locations is as follows:

1) 5th Location (1.060)
2) 1st Location (0.942)
3) 2nd Location (0.911)
4) 3th Location (0.435)
5) 4th Location (0.203)

4.1.3 International Friction Index

The PIARC model is the basis of the definition of the International Friction Index, IFI, through the parameters F60 and Sp. Thus, the IFI of a pavement is expressed by the pair of values (F60, Sp) expressed in parentheses and separated by a comma; the first value represents the friction

and the second the macrotexture.

The first is a dimensionless number and the second is a positive number with no limits and with units of speed (km/h). The friction zero value indicates perfect slip and the value one, grip. For the moment it is not possible to describe with a simple relation the second number that makes up the IFI. [52]

During the elaboration of the model, and from the data of the PIARC experiment, it has been verified that the velocity constant Sp can be determined by means of a linear regression in function of the field measurement of the macrotexture (TX).

The representative Sp and F60 values obtained using Equations (7) to (9) are replaced for each section given. Once these parameters have been calculated, and using (10), the estimated friction values F for the velocity of time are calculated. These values are presented in Table 8, and the behavior curves of the pavement surface are plotted as shown in Figure 22.

Table 8 – Calculation of IFI

	TX	Sp	Friction	F(s) values, km/h						
	(mm)	(km/hr)	(S.R.C)	0	20	40	60	80	100	120
1st Loc	0.942	95.47	0.564	0.606	0.491	0.399	0.323	0.262	0.213	0.172
2nd Loc	0.911	91.93	0.633	0.672	0.541	0.435	0.350	0.282	0.227	0.182
3rd Loc	0.435	37.87	0.531	0.826	0.487	0.287	0.169	0.100	0.059	0.035
4th Loc	0.203	11.50	0.521	11.346	1.992	0.350	0.061	0.011	0.002	0.000
5th Loc	1.060	108.90	0.507	0.542	0.451	0.375	0.312	0.260	0.216	0.180

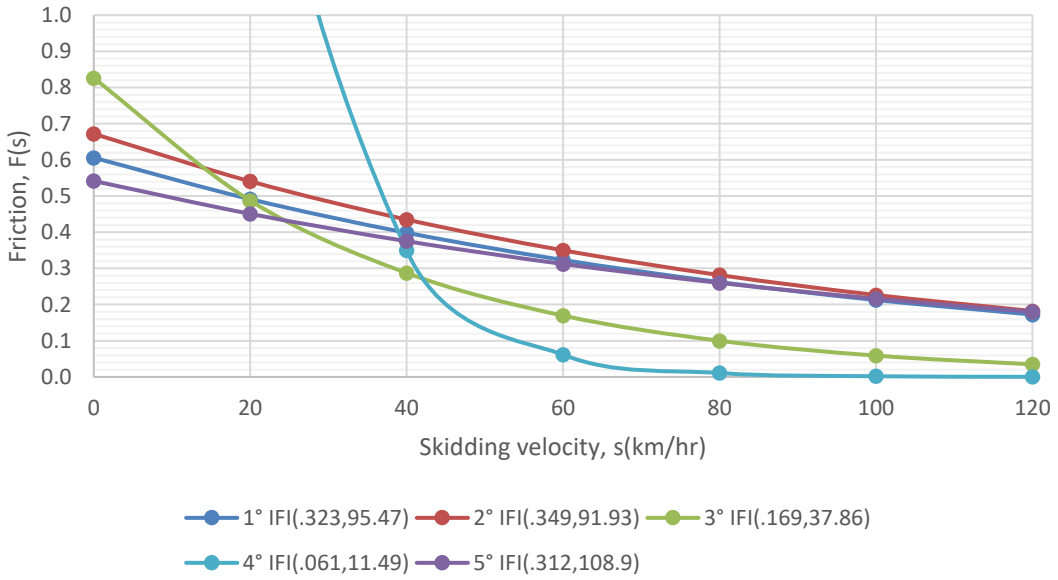

Figure 22 - Comparison of sections with IFI (F60, Sp)

In this graph it can be observed that at a higher speed the friction is decreasing, this is due to the reduction of the contact area between the pneumatic-pavement interface.

4.1.4 Acceptance/Rejection Graph

Now the acceptance/rejection graph for each location is presented, which is going to indicate if each of the sections under study have the proper characteristics of friction and texture. Using the acceptance/rejection graph of Figure 10 as reference, where each segment is divided according to its quality. The graph with the five location points measured is evaluated in Figure 23. [15]

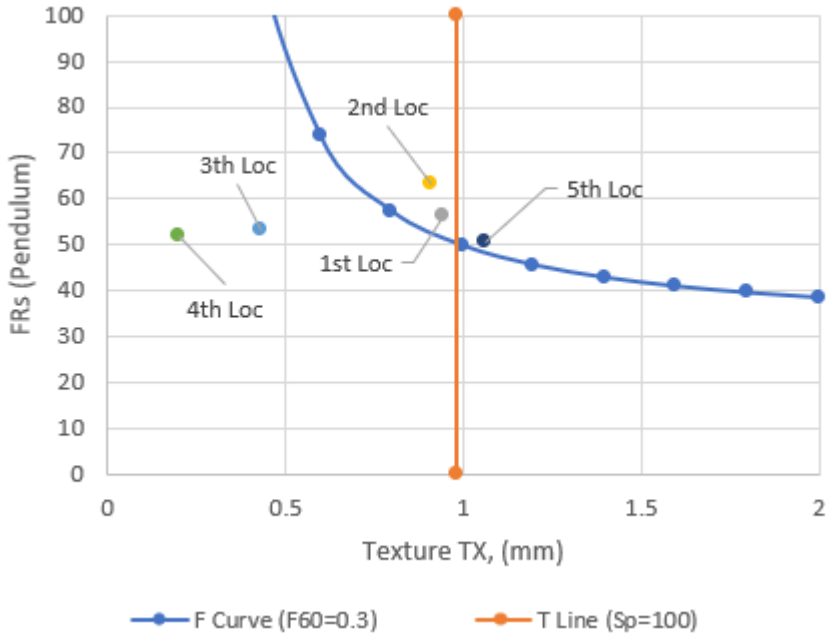

Figure 23 – Acceptance/Rejection curve for the five locations

According to Fig. 23, we observe an open texture in Locations 1,2 and 5, since the pavement has a seal irrigation (correctly applied), which affects the value of Sp giving an average around 100 km/h.

On the other hand, we observe a closed texture at locations 3 and 4, giving the value of Sp an average below 40 km/h, also presenting a low friction due to the use of stony material of calcareous origin, which produces an accelerated polishing of the surface. Location 5 also present low friction due to the use of stone material of calcareous origin.

Location 1 present more friction because there is a lower number of vehicles passing over, and Location 2 present more friction because the pavement has less than a month of renewal before making the experimentation.

As previously seen in Chapter 2, for road quality evaluation purposes the Mexican government suggested Table 3 for friction values measured with the British pendulum in wet pavement

(critical condition) and Table 4 for macrotexture values with the Sand patch test in dry pavement.

It is possible to notice that the tables proposed by the Mexican government are more flexible with values when comparing with the acceptance/rejection graph. According to this criterion, all the friction values measured are very good with exception of Location 5, which is considered just as good. With respect to texture, Location 1, 2 and 5 are considered very good, Location 3 as bad, and 4 as prohibited.

4.2 Measurement with Acoustic System

4.2.1 Description

Afterwards, measurements were made at the same points of the city, but now with the acoustic system for its characterization. The measurements were carried out at a temperature of 27°C and at an atmospheric pressure of 947 hPa.

The following equipment was used: two small omnidirectional microphones, with frequency response of 20-20,000 Hz; small directional speaker with frequency response of full range; audio interface of 2 channels, with sampling frequency of 96 kHz; a laptop and software for signal processing.

The purpose of this work was to measure the sound level difference of two microphones, positioned at heights Ht (height of top microphone) and Hb (height of bottom microphone) when a loudspeaker radiates a MLS signal from a horizontal distance d to the microphones, and a height Hs, (height of source). The parameters of a ground impedance model were modified and compared with the experimental curve. The difference in the impedance of the soil between the experimental and the theoretical curves is minimized [16].

The ANSI S1.18 Standard proposes three geometries: A, which covers a wider range of frequencies, B, which emphasizes the effect of the ground at frequencies above 1000 Hz, and is recommended for hard soils, and C which highlights the effect of the soil at frequencies below 1000 Hz, and should be used for soft grounds. The ANSI S1.18 standard covers a frequency range of 250–4 kHz. It recommends using a signal with level at least 10 dB above the background noise level. In any case, you should use windscreens for microphones. The soil must be flat. We accomplished the recommendations of the standard.

Kruse and Mellert [17] recommended a slightly different geometry, obtained after an error minimization process in the frequency range between 100 and 400 Hz. But in this case, we use different geometry, obtained after a geometry optimization process in the frequency range between 0.3 and 7 kHz, due to the experimental conditions.

4.2.2 Static Measurements

For all the measurements along different avenues, two microphones were mounted on a support base at different heights from the soil: 0.065 m and 0.165 m; the source was at a height of 0.165 m, and the distance between microphones and speaker was 0.45 m. Figure 24 presents a schematic representation of the static system.

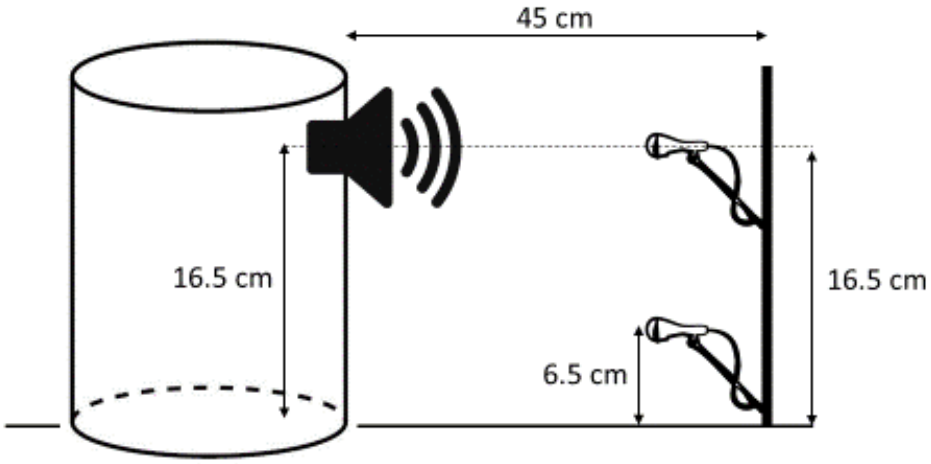

Figure 24 – Static system

MLS signals of order 18 were used, with 3 averages, and sample frequency of Fs = 96 kHz. Figure 25 shows the experimental setup and the ground patch of asphalt to perform the characterization. The source can be seen oriented in the direction of the support holding the two microphones.

Figure 25 – Acoustic measurement at the 1st location

The results obtained from this experimentation are presented in Table 9 for the four parameters measured, obtaining different acoustic properties such as flow resistivity, rate of change of porosity, porosity, tortuosity, and shape factor at the five locations. It is important to notice that the original values obtained were the ones reported, cause since the measurements were made in a static position, there was not much noise interference.

Table 9 – Acoustic parameters measured with static system

	1 Parameter				
	1st Location	2nd Location	3th Location	4th Location	5th Location
	Original	Original	Original	Original	Original
flow resistivity	1,494,105	1,025,143	1,483,883	2,216,315	1,191,020
	2 Parameters				
	1st Location	2nd Location	3th Location	4th Location	5th Location
	Original	Original	Original	Original	Original
flow resistivity	400,000	496,577	573,691	1,472,751	613,989
rate of change of porosity	159	1	250	1	1
	3 Parameters				
	1st Location	2nd Location	3th Location	4th Location	5th Location
	Original	Original	Original	Original	Original
flow resistivity	1,697,344	489,764	1,697,638	561,861	618,313
porosity	0.9	0.4375	0.9	0.2932	0.4154
tortuosity	1	1.5588	1	6.0356	1
	4 Parameters				
	1st Location	2nd Location	3th Location	4th Location	5th Location
	Original	Original	Original	Original	Original
flow resistivity	2,890,611	929,385	2,682,770	440,033	957,345
porosity	0.9	0.3960	0.9	0.1184	0.4171
tortuosity	1	2.075	1	1.449	1.034
shape factor	0.4834	0.4379	0.4991	0.4860	0.4963

To understand and compare the results graphically, Figure 26 shows the comparison between the flow resistivity for the four parameters measured. Comparisons between porosity and tortuosity for 3 and 4 parameters are also presented in Fig. 27 and 28 respectively for the five locations.

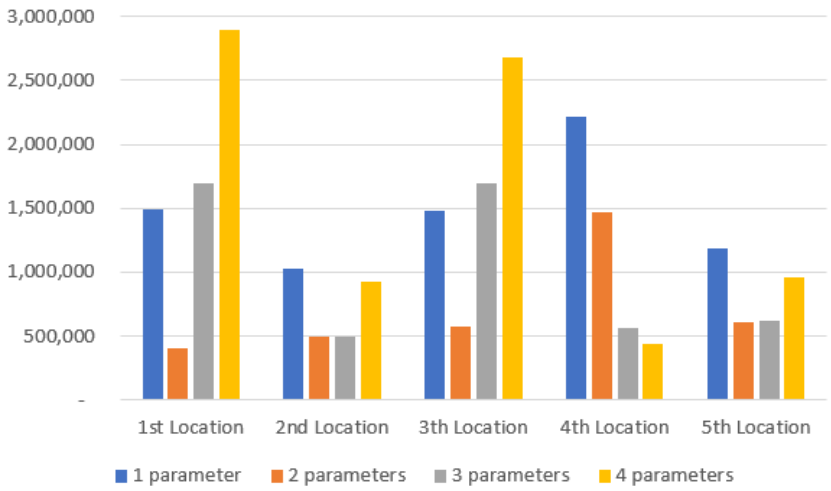

Figure 26 - Comparison of flow resistivity for 1 to 4 parameters

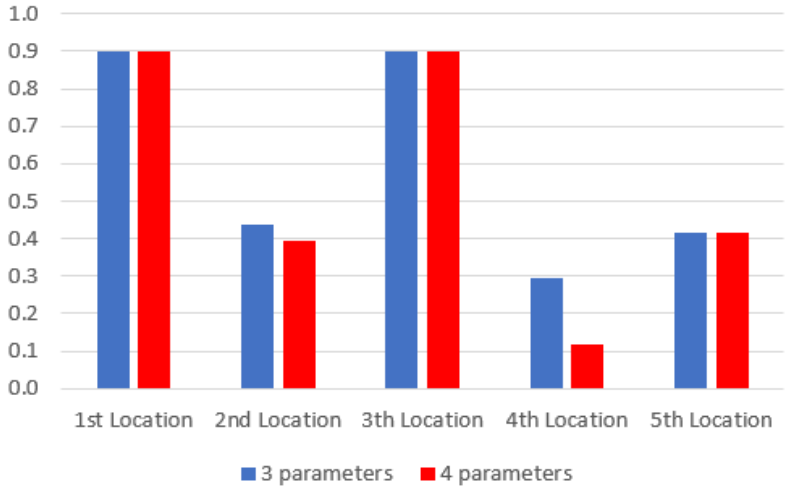

Figure 27 - Comparison of porosity for 3 and 4 parameters

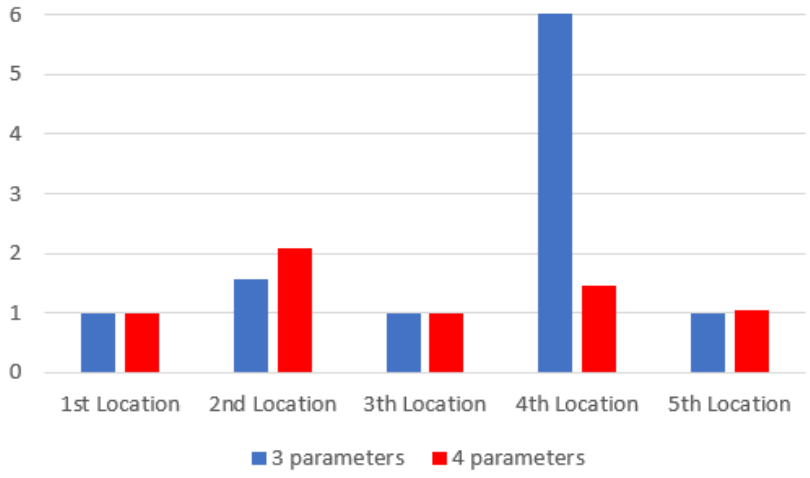

Figure 28 - Comparison of tortuosity for 3 and 4 parameters

4.2.3 Dynamic Measurements

For data collection purposes, a 2005 Nissan Xterra with an inexpensive microphone in front of the rear tire was instrumented, as shown in Fig. 29. The gain level of the microphone and its distance from the tire were kept the same for the entire data collection process. Five different routes were selected. For each route, the same exact path was driven when the road surface was completely dry, as shown in Fig. 30. The duration and length of the trips were 120 min, around 3 km distance, and an average speed of 40 km/h when taking the measurements.

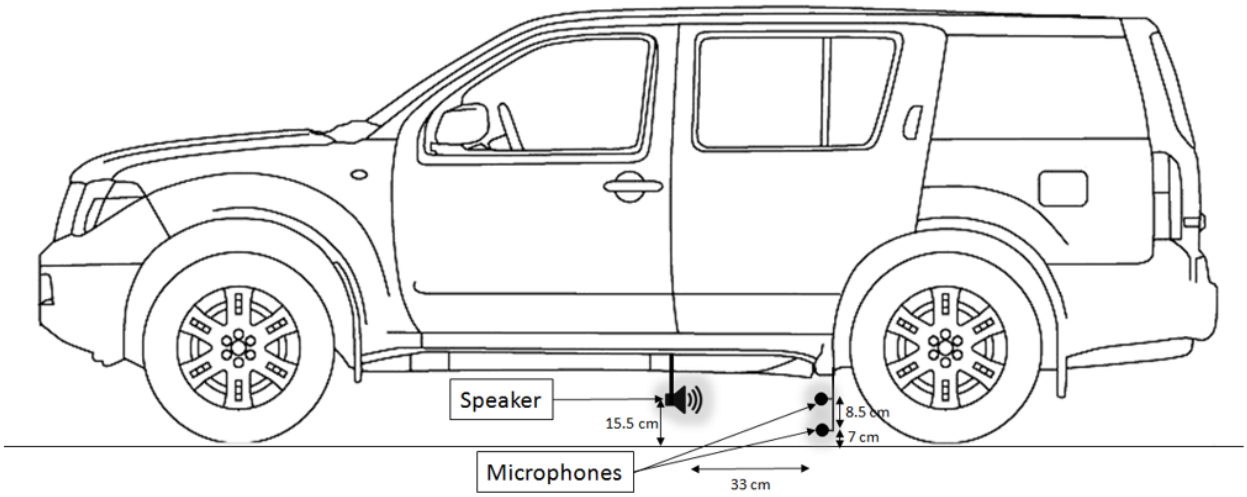

Figure 29- Representation of the acoustic system mounted on the car

Figure 30 - Acoustic system mounted at the front of the driver's rear tire

The data collection was carried out in the southern Monterrey area with different speeds, traffic conditions and pavement roughness. Our dataset contains values from 0 km/hr to 40 km/hr. The route traveled is a combination of surface-treated road and bituminous concrete road.

The summary of the dataset is presented on Table 10 for the four parameters measured,

obtaining different acoustic properties such as flow resistivity, rate of change of porosity, porosity, tortuosity, and shape factor at the five locations. It is important to notice that the windowed values obtained were the ones reported, cause since the measurements were made under movement and traffic, there was noise interference which had to be filtered.

Table 10 – Acoustic parameters measured with dynamic system

	1 Parameter				
	1st Location	2nd Location	3th Location	4th Location	5th Location
	Windowed	Windowed	Windowed	Windowed	Windowed
flow resistivity	4,879,054	2,167,458	1,133,702	770,843	1,606,417
	2 Parameters				
	1st Location	2nd Location	3th Location	4th Location	5th Location
	Windowed	Windowed	Windowed	Windowed	Windowed
flow resistivity	3,025,464	988,448	1,393,736	400,000	1,072,664
rate of change of porosity	1	1	1	1	1
	3 Parameters				
	1st Location	2nd Location	3th Location	4th Location	5th Location
	Windowed	Windowed	Windowed	Windowed	Windowed
flow resistivity	400,000	400,000	400,000	400,000	400,000
porosity	0.30308	0.49032	0.56049	0.9	0.53887
tortuosity	10	10	10	5.2086	10
	4 Parameters				
	1st Location	2nd Location	3th Location	4th Location	5th Location
	Windowed	Windowed	Windowed	Windowed	Windowed
flow resistivity	400,000	400,000	426,672	450,517	400,000
porosity	0.51262	0.4688	0.4455	0.55867	0.53851
tortuosity	10	10	6.9715	5.4443	10
shape factor	0.1	0.1	0.15289	0.26919	0.1

To understand and compare the results graphically, in Figure 31 the is a comparison between the flow resistivity for the four parameters measure. Comparisons between porosity and tortuosity for 3 and 4 parameters are also presented in Fig. 32 and 33 respectively for the five locations.

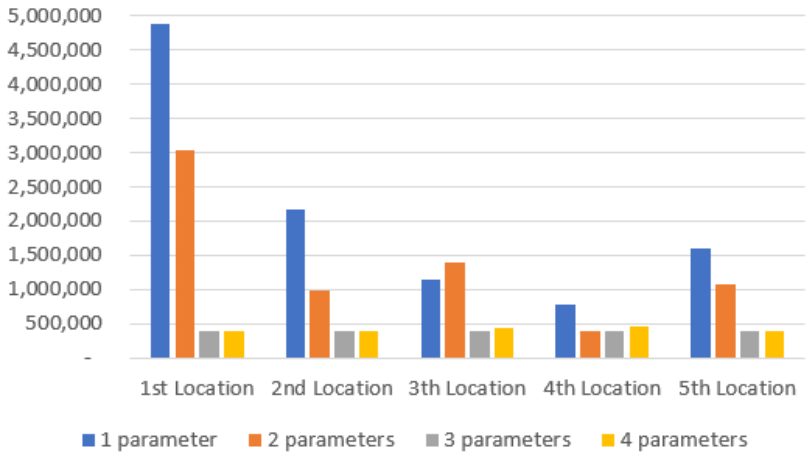

Figure 31 - Comparison of flow resistivity for 1 to 4 parameters

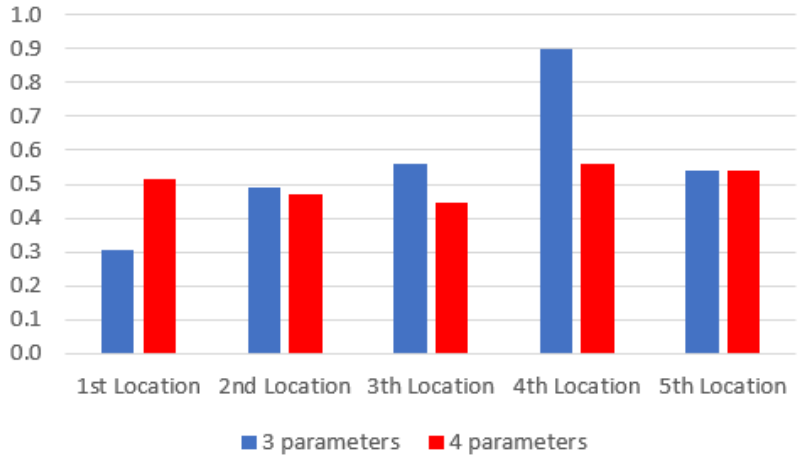

Figure 32 - Comparison of porosity for 3 and 4 parameters

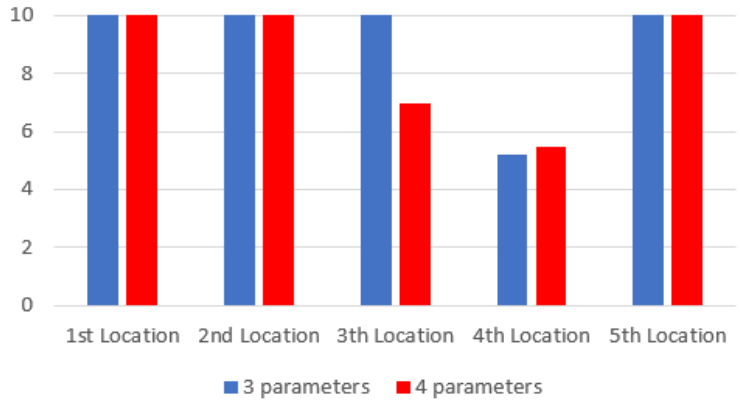

Figure 33 - Comparison of tortuosity for 3 and 4 parameters

Chapter 5

Results

5.1 Relationship between mechanical and acoustical parameters

5.1.1 Static Measurements

As said before, the values reported for the static system graphs were the original values, because for these measurements there was a relatively controlled environment for the noise in the experimentation.

From the acoustic parameters, it was decided to stay with the porosity because it presented the highest similarity between 3 and 4 parameters, as previously seen in Figure 27. After obtaining the correlation coefficient (r) between TX, S.R.C., and IFI against porosity, also seen in Table 11, it was founded that IFI is the variable with the strongest correlation for both porosity parameters.

Table 11 – Static system correlation coefficient (r) comparison.

	Porosity	
	3 parameters	4 parameters
TX	0.1745	0.1771
S.R.C.	0.0637	0.0184
IFI	0.2614	0.2518

Figures 34 and 35 show the linear correlation between IFI and Porosity, where the linear regression equation (y) and the coefficient of determination (r^2) are also displayed on the graphs.

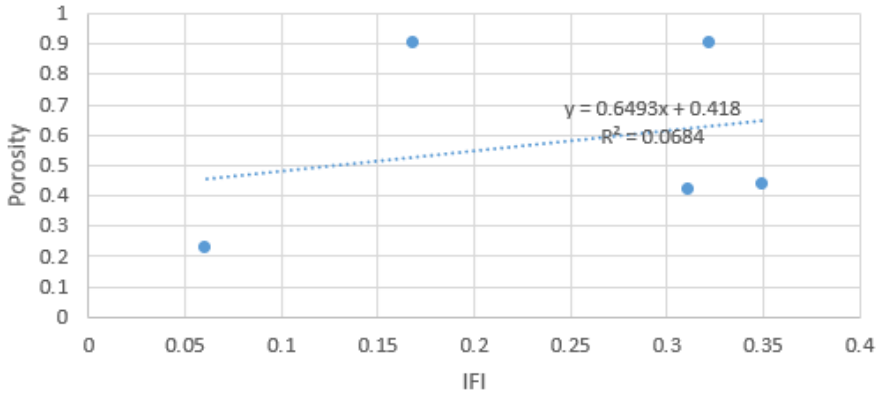

Figure 34 - Correlation between IFI and Porosity with 3 parameters. (r=0.26)

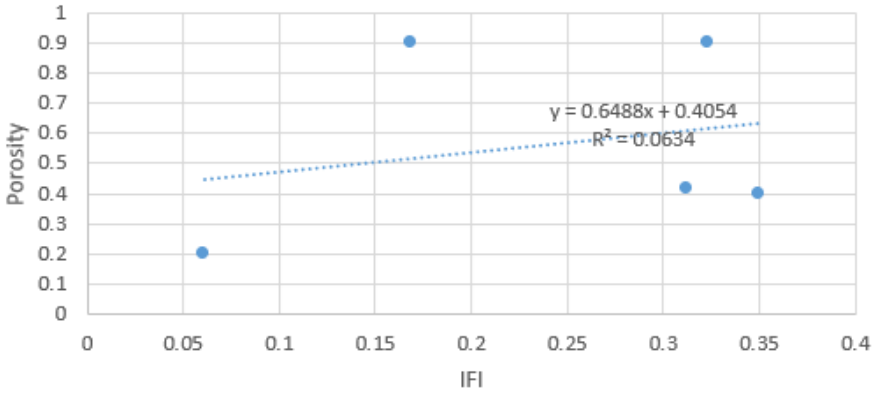

Figure 35 - Correlation between IFI and Porosity with 4 parameters. (r=0.25)

From these results it is seen that for both porosity 3 and 4 there is a weak positive relationship with respect to IFI, since the correlation coefficients are r=0.26 and 0.25 respectively.

5.1.2 Dynamic Measurements

As previously said, the values reported for the dynamic system were the windowed values, because since these measurements were taken with the car in motion, the influence of the environmental noise played a huge role and had to be diminished by using a filtering postprocess.

From the acoustic parameters, it was also decided to stay with the porosity because of the high similarity between 3 and 4 parameters, as previously seen in Figure 32. After obtaining the correlation coefficient (r) between TX, S.R.C., and IFI against porosity, also seen in Table 12, it was founded that IFI has a very strong correlation for 3 parameters but a weak one for 4, meanwhile Friction (S.R.C.) has a strong correlation for both porosity parameters.

Table 12 – Dynamic system correlation coefficient (r) comparison.

	Porosity	
	3 parameters	4 parameters
TX	-0.7911	-0.0661
S.R.C.	-0.4213	-0.5013
IFI	-0.8543	-0.2704

Figures 36 and 37 show the linear correlation between IFI and Porosity, where the linear regression equation (y) and the coefficient of determination (r^2) are also displayed on the graphs.

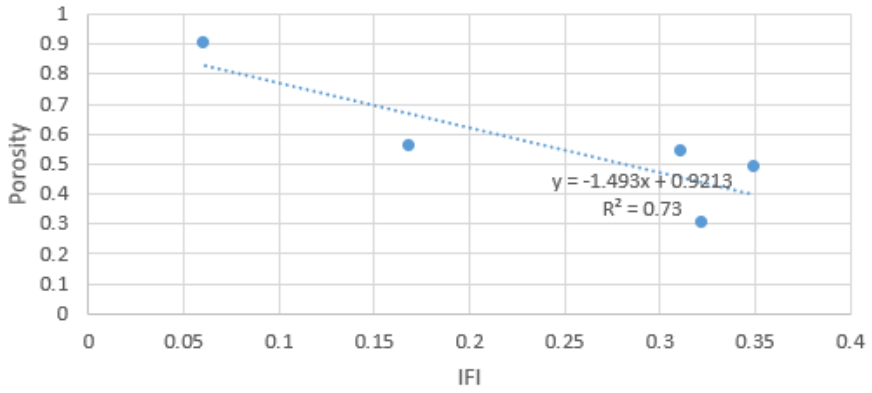

Figure 36 - Correlation between IFI and Porosity with 3 parameters (r=-0.85)

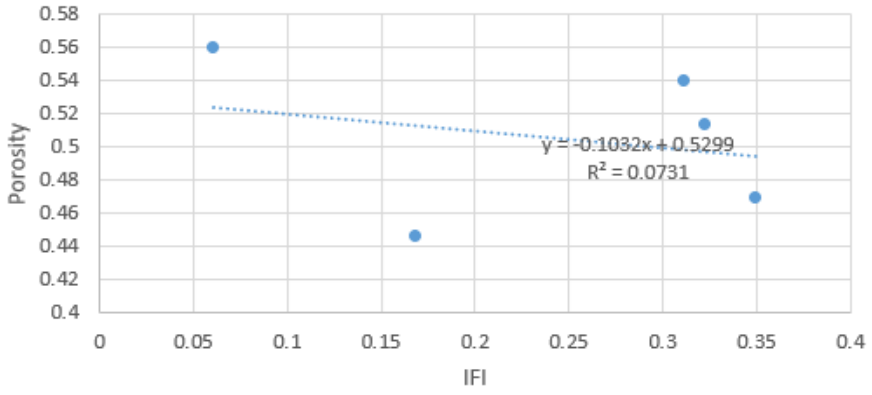

Figure 37 - Correlation between IFI and Porosity with 4 parameters (r=-0.27)

From these results it is observed that for IFI vs porosity 3 there is a strong negative relationship, since r=-0.85, but on the other hand, there is a weak negative relationship between IFI and porosity 4, since r=0.27.

The linear correlation between Friction (S.R.C.) and Porosity is shown in Figures 38 and 39, where the linear regression equation (y) and the coefficient of determination (r^2) are also displayed on the graphs.

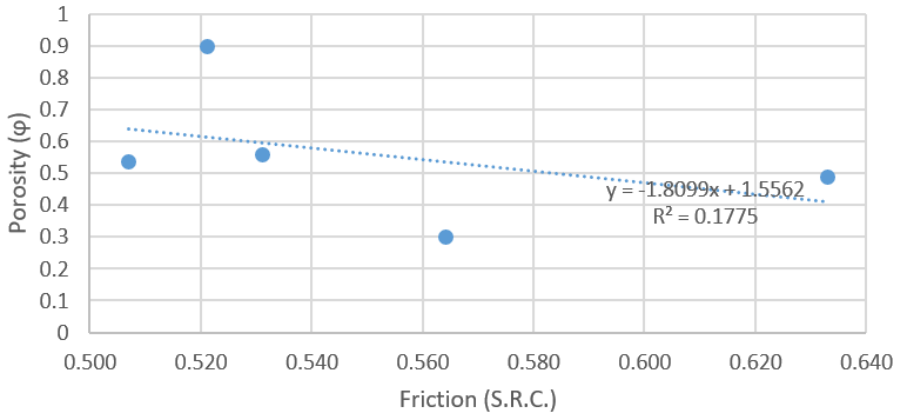

Figure 38 - Correlation between Friction and Porosity with 3 parameters (r=-0.42)

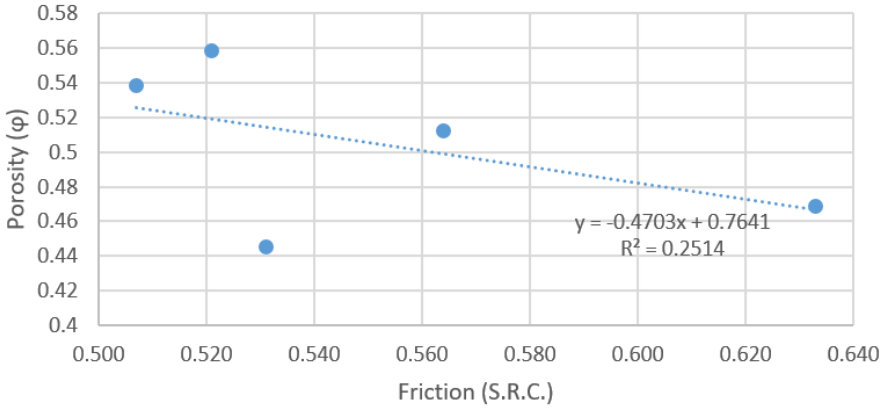

Figure 39 - Correlation between Friction and Porosity with 4 parameters (r=-0.5)

From these results it is observed that for both porosities 3 and 4 there is a strong negative relationship with respect to Friction (S.R.C), since the correlation coefficients are r=0.42 and r=-0.5 respectively.

.

Chapter 6

Conclusions

6.1 Contributions

An approach based on acoustic signals for detecting road characteristics from audio of the surface-tire interaction was proposed. The method shows to be robust to vehicle speed, road type, and pavement quality. As seen along the thesis, the advantages of using acoustic sensors to measure the characteristics of the asphalt compared to other types of sensors are its low cost, portability and capacity to work even at high velocities.

Advantages of the acoustic system in comparison to optical sensors, are that precision of optical sensors diminishes significantly under low visibility conditions as night or fog, and that its image processing packages are very expansive in comparison to the acoustic equipment.

Ultrasonic sensors work well when working with fluids, but for the purpose of the thesis, the acoustic sensor would suit better for the application of the road surface characterization.

Limitations of using acoustic device are that even though environmental noise could be filtered, extreme noise or reflections could affect the results of the measurements. Extreme weather conditions must be also tested, since heavy rain could also create unwanted noise on the measurements.

From the results obtained several conclusions are made. The first experimentation done with the impedance tube used to prove that there is a very strong negative relationship between the acoustical absorption and the friction (S.R.C.) measured with the impedance tube, which was the first step to continue with the main experimentation using the acoustic system.

The main experimentation using the acoustic system was divided into the static and the dynamic characterization. The static characterization showed a weak positive relationship between IFI vs porosity, and for the dynamic system a strong negative relationship between IFI vs porosity and also between Friction (S.R.C.) vs porosity was obtained.

Since both the impedance tube and the dynamic system showed a strong negative correlation, meanwhile the static system showed just a weak positive correlation, it is likely to say that the acoustic characterization is validated, but more measurements are necessary to obtain better results.

The negative correlation relationship means that the higher the Acoustic Absorption or Porosity, the lower the IFI or Friction (S.R.C.) available, and the other way around. This could be also explained as following:

α or $\varphi = 1 \rightarrow$ The highest acoustic absorption or porosity, the least friction available, and the least adhesion to the road.

α or $\varphi = 0 \rightarrow$ The least acoustic absorption or porosity, the highest friction available, and the highest adhesion to the road.

6.2 Future work

For future work, the acoustic system could classify the type of soil into dry, wet, snowy or icy asphalt depending on its real-time conditions by interpreting the acoustic absorption or porosity of the road surface. For this purpose, it is necessary to expand the experimentation with different vehicle dimensions, weather conditions, and type of soils.

A potential automotive application for the acoustic system developed will be to connect it to the car and start making tests on how the performance of the Anti-Lock Braking system (ABS) is improved with the addition of the acoustic system. A detailed explanation of this automotive application and two others are now explained.

Anti-Lock Braking System Application

The ABS has the function of maintaining the wheel slip between desired ranges. The ECU (Electronic Control Unit) is the device in charge of controlling the blocking tires. The performance in the vehicle velocities and the wheel slip is related with the parameters of the ABS model and on the terrain conditions (coefficient of friction) where the test is performed. The system not only decelerates optimally, but also maintains a better control of direction and stability on the vehicle.

A typical system of the vehicle control is monitoring continuously the angular velocity of the wheels [47]. Whenever an initial blocking tire is detected, the central unit adopts the maintenance phase of the hydraulic pressure in the brake caliper of the correspondent wheel. Pressure maintenance is achieved by switching the inlet valve of the hydraulic modulator of the anti-lock braking system. As the locking tendency disappears, the control unit allows a further increase of pressure until the wheel tends again to lock; an ABS system is depicted in Figure 40. This sequence is repeated continuously until the driver stops pushing the brake or the wheel tends to lock. In such a case, the electronic brake distribution stops acting to give way to the anti-lock function that allows the reduction of the pressure on the brakes.

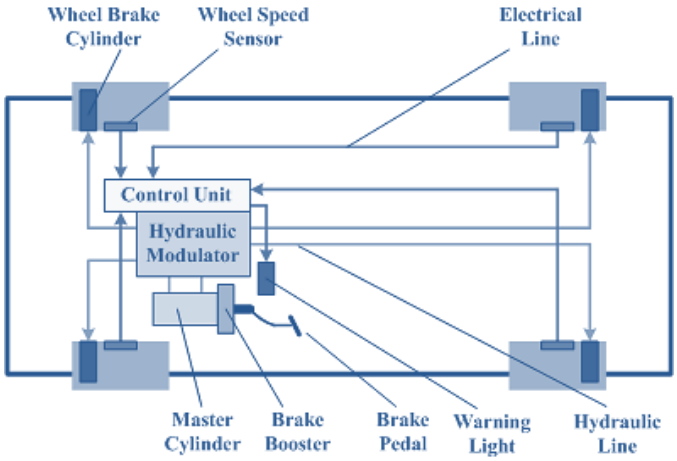

Figure 40 - ABS System.

A typical ABS system seeks to prevent the tires from locking and at the same time keep the slip within a desirable range (usually between 10% and 30%) so as not to lose control of the vehicle [48]. This system not only decelerates optimally but also allows better control of the steering and stability of the vehicle, but how would it work under panic situations especially when the slip conditions may vary like the image in Figure 41.

When the tires are locked, the braking and cornering coefficients become sliding. Modern ABS systems work on the low-slip side of the friction curve. The car may just go spinning if the slip suddenly develops or if the surface is wet. With ABS, the tires are being braked with slip continuously calculated.

However, it is still hypothesized that its operation can be improved by maintaining the optimum sliding range for each type of soil, since the behavior of the system changes depending on the pavement conditions.

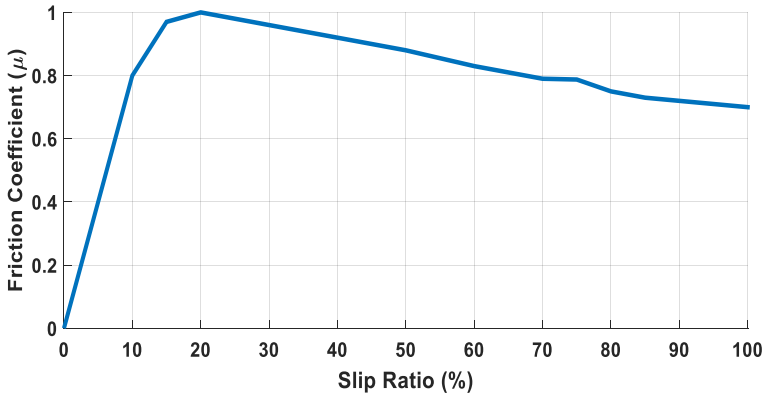

Figure 41 - Braking slip effect on friction coefficient vs. wheel slip

The workflow of the implementation is explained in Fig. 42, which show a schematic flow diagram of the system, which will work by improving the vehicle control using an acoustic sensor.

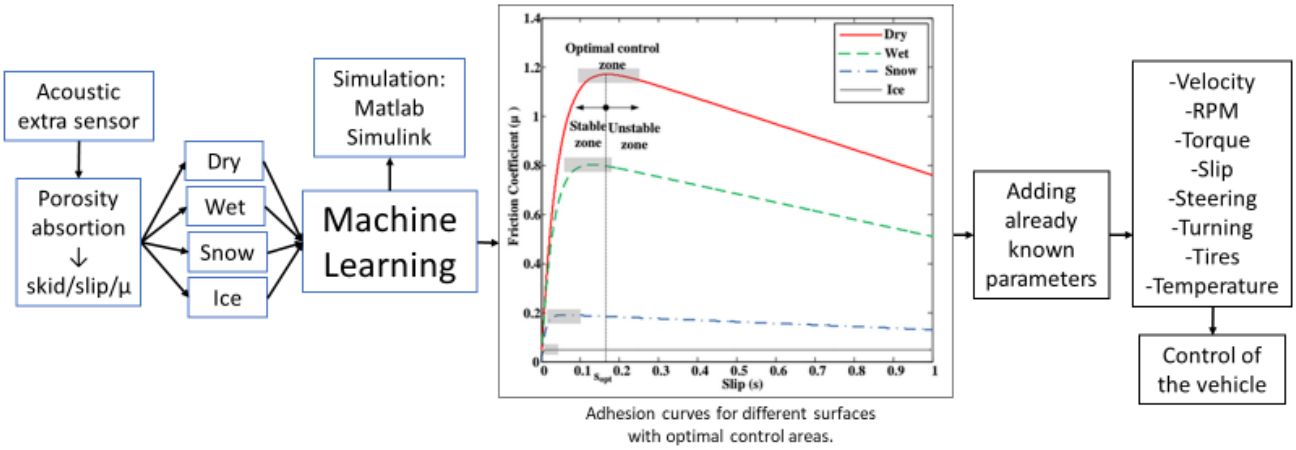

Figure 42 - Work flow of the implementation.

The ABS Braking Model presented by MathWorks was implemented for the simulation of the ABS system [21]; it is shown in Fig. 43. The model is based in a quarter of a vehicle, or respectively to one wheel. This model simulates the dynamic behavior of the vehicle under severe braking conditions. This can be replicated countless times to create a model of a multi-wheel vehicle.

The design of the ABS control circuit is widely based on vehicle dynamics, and more specifically on the contact analysis between the wheel and the road, as presented on this work.

The model maintains the slip of the vehicle in a desired value, which is considered depending on the type of surface. For this reason, a test of the system working in Matlab/Simulink was developed. The model is analyzed to develop a control technique more accurate for the ABS systems.

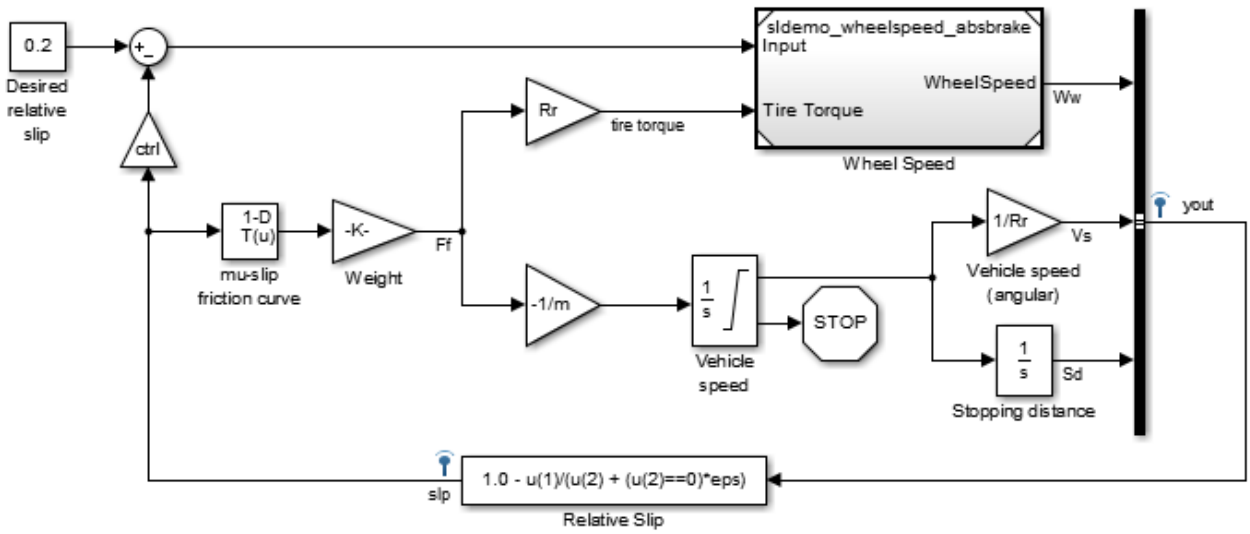

Figure 43 – Elements of an Anti-Lock Braking System (ABS) model

The elements of this model represent the performance and advantages of the ABS systems in a passenger vehicle.

A vehicle will always present a sliding percentage because of the friction force generated by the interaction tire-ground. An adequate range stablished by Wong [4] is proposed between 10 and 30%, so that is why a value of 20% is selected between the optimum range, but this will depend on the type of ground by which the car transits. This value is the reference of the control diagram, and it is lower as the number of revolutions on the wheel, which is 0.8 times the number of revolutions under braking conditions, for the same velocity of the vehicle. This maximizes the adhesion between the road and the tire and minimizes the distance of braking with the available coefficient of friction.

Other Automotive Applications

Other future automotive applications will be to display a slippery condition warning on the driver's dashboard indicator light, as seen in Figure 44, or to send this information to autonomous cars to improve the driving behavior of the vehicle when slippery conditions are present, as shown in Figure 45.

Figure 44 – Slippery Condition Warning

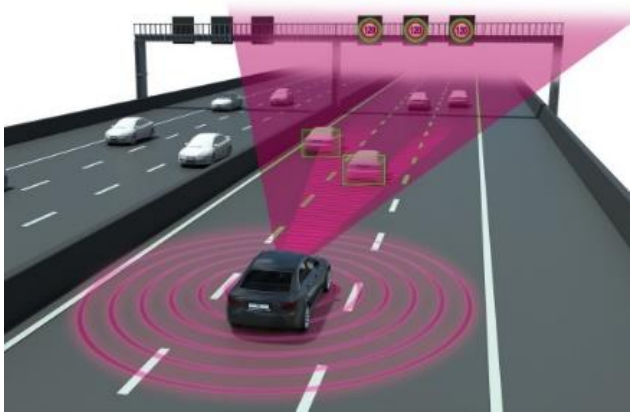
Figure 45– Automated driving system

Bibliography

[1] M. Mueller, “Sensor sensibility: Advanced driver assistance systems,”Vision Zero International, 2015.

[2] J. Alonso, J. López, I. Pavón, M. Recuero, C. Asensio, G. Arcas, and A. Bravo, “On-board wet road surface identification using tyre/road noise and support vector machines,” Applied Acoustics, vol. 76, pp. 407–415, 2014.

[3] Baffet G., Charara A., Lechner D., Thomas D. (2007). An Estimation Process for Tire-Road Forces and Sideslip Angle for Automotive Safety Systems. Informatics in Control, Automation and Robotics pp 125-138.

[4] (INEGI), Instituto Nacional de Estadítica y Geografía. Accidentes de tránsito terrestre en zonas urbanas y suburbanas. 2017. https://www.inegi.org.mx/sistemas/olap/proyectos/bd/continuas/transporte/accidentes.asp. 03 12 2018.

[5] Rievaj, V., Vrábel, J., & Hudák, A. (2013). Tire Inflation Pressure Influence on a Vehicle Stopping Distances, 2(2), 9–13. https://doi.org/10.5923/j.ijtte.20130202.01

[6] UK Department of Transport. General rules, techniques and advice for all drivers and riders (103 to 158). 1 10 2015. https://www.gov.uk/guidance/the-highway-code/general-rules-techniques-and-advice-for-all-drivers-and-riders-103-to-158#rule126.

[7] Ministry of Transportation and Infrastructure Online. Why Stopping Distances Matter More During the Winter. 11 2017. https://www.tranbc.ca/2016/12/16/why-stopping-distances-matter-more-during-the-winter/.

[8] Physics, American Institute of. Sound medicine at Acoustics Meeting. 13 11 2007. https://www.eurekalert.org/pub_releases/2007-11/aiop-sma_1111307.php.

[9] Kuttesch, J. S., Trani, A., & Kuttesch, J. S. (2004). Quantifying the Relationship between Skid Resistance and Wet Weather Accidents for Virginia Data Quantifying the Relationship between Skid Resistance and Wet Weather Accidents for Virginia Data.

[10] Targeted, S., & Project, I. (2006). Specific targeted research or innovation project: Integrated Tire and Road Interaction – ITARI Deliverable 5.1: Development of a Tire-Road Friction Model.

[11] Smith, K. L. (2009). National Academies of Sciences, Engineering, and Medicine. Guide for Pavement Friction. Washington, DC: The National Academies Press.

[12] TYROSAFE (2008-2010): Tyre and Road Surface Optimisation for Skid resistance and Further Effects (FP7, Transport Call 2007).

[13] Panagouli, O.K., and Kokkalis, A.G. (1998). Skid Resistance and Fractal Structure of Pavement Surface. Chaos, Solutions & Fractals, 9(3), 493-505.

[14] H., Carlos Kraemer. Firmes. Madrid: Escuela Politécnica de Madrid, 1990.

[15] Diana Berenice López Valdéz. Consideraciones para la aplicación del índice de fricción internacional en carreteras en México. Research Paper. Sanfandila, Querétaro: Technical Publication No. 170, 2001. Document.

[16] Bohdan T. Kulakowsky, John J. Henry, Chunming Lin. "A closed loop Calibration Procedure for a British Pendulum Tester." Meyer, W. E. Surface Characteristics of Roadways: International Research and Technologies. Philadelphia: ASTM, 1990. 103-105. Document.

[17] Rodríguez, Carlos Humberto Fonseca. Medición del índice de fricción internacional, IFI, en superficies de rodamiento del área metropolitatan de monterrey para definir las áreas con mayor índice de accidentes. Local pavement assessment. Monterrey: ITESM, 2009.

[18] Method, S. T. (2018). Standard Test Method for Measuring Pavement Macrotexture Depth Using a, 15–18. https://doi.org/10.1520/E0965-15.2

[19] Instituto Mexicano del Transporte. Diagnóstico de las características superficiales de los pavimentos. Sanfandilla, Querétaro: Technical Publication No. 111, 1998.

[20] Rodríguez, Dr. Carlos Humberto Fonseca. Medición del índice de fricción internacional, IFI, en superficies de rodamiento del área metropolitana de monterrey para definir las áreas con mayor índice de accidentes. Report. Monterrey: ITESM, 2008. Document.

[21] Russon, Mary-Ann. International Business Time. 8 December 2015. https://www.ibtimes.co.uk/heres-how-self-driving-cars-can-detect-dangerous-roads-using-sound-ai-1532407

[22] Abdić, I., Fridman, L., Marchi, E., Member, S., Brown, D. E., Angell, W., & Reimer, B. (2015). Detecting Road Surface Wetness from Audio: A Deep Learning Approach, (1), 1–5.

[23] Y. Horita, S. Kawai, T. Furukane, and K. Shibata, “Efficient distinction of road surface conditions using surveillance camera images in night time,” in Image Processing (ICIP), 2012 19th IEEE International Conference on. IEEE, 2012, pp. 485–488.

[24] Ibarra, D., Ramírez-mendoza, R., & Ibarra, S. (2016). Characterization of the road surfaces

in real time. Applied Acoustics, 105, 93–98.

[25] P. Jonsson, J. Casselgren, and B. Thornberg, “Road surface status classification using spectral analysis of nir camera images,” Sensors Journal, IEEE, vol. 15, no. 3, pp. 1641–1656, 2015.

[26] V. V. Viikari, T. Varpula, and M. Kantanen, “Road-condition recognition using 24-ghz automotive radar,” Intelligent Transportation Systems, IEEE Transactions on, vol. 10, no. 4, pp. 639–648, 2009.

[27] K. Iwao and I. Yamazaki, “A study on the mechanism of tire/road noise,” JSAE review, vol. 17, no. 2, pp. 139–144, 1996.

[28] M. Bao, C. Zheng, X. Li, J. Yang, and J. Tian, “Acoustical vehicle detection based on bispectral entropy,” Signal Processing Letters, IEEE, vol. 16, no. 5, pp. 378–381, 2009.

[29] R. Birken, G. Schirner, and M. Wang, “Voters: design of a mobile multimodal multi-sensor system,” in Proceedings of the Sixth International Workshop on Knowledge Discovery from Sensor Data. ACM, 2012, pp. 8–15.

[30] L. Fridman, D. E. Brown, W. Angell, I. Abdi´c, B. Reimer, and H. Y. Noh, “Automated synchronization of driving data using vibration and steering events,” arXiv preprint arXiv:1510.06113, 2015.

[31] Li, K.M., Waters-Fuller, T., Attenborough, K., 1998. Sound propagation from a point source over extended-reaction ground. J. Acoust. Soc. Am., 104: 679-685.

[32] Mechel FP. Formulas of acoustics. Berlin: Springer Verlag; 2008.

[33] Ibarra D, Cobo P, Anfosso-Lédée F. Relationship between the noise radiated by a vehicle to the near and the far fields. Noise Cont Eng J 2013;61: 446–57.

[34] Delany ME, Bazley EN. Acoustical properties of fibrous absorbent materials. Appl Acoust 1970; 3:105–16.

[35] Ibarra D, Ramirez-Mendoza R, Lopez E, Bustamante R. Influence of the automotive Start/Stop system on noise emission: experimental study. Appl Acoust 2015; 100:55–62.

[36] Faure, O., Gauvreau, B., Junker, F., Lafon, P., & Bourlier, C. (2017). Modeling of random ground roughness effects by an effective impedance and application to time-domain methods. Applied Acoustics, 119, 1–8. https://doi.org/10.1016/j.apacoust.2016.11.019

[37] Boulanger P, Attenborough K, Taherzadeh S, Waters-Fuller T, Li KM. Ground effect over hard rough surfaces. J Acoust Soc Am 1998;104(3):1474–82.

[38] Rienstra S. Impedance models in time domain including the extended Helmholtz resonator model. In: Proceedings 12th AIAA/CEAS aeroacoustics conference, Cambridge MA, USA, May 8 10, 2006, vol. 2686; 2006. p. 1 [Paper AIAA 2006].

[39] Dragna D, Blanc-Benon P. Physically admissible impedance models for time-domain computations of outdoor sound propagation. Acta Acust United Acust 2014;100(3):401–10.

[40] Kirby R. On the modification of Delany and Bazley fomulae. Appl Acoust 2014; 86:47–9.

[41] Dragna D, Attenborough K, Blanc-Benon P. On the inadvisability of using single parameter impedance models for representing the acoustical properties of ground surfaces. J Acoust Soc Am 2015;138(4):2399–413.

[42] Attenborough K, Bashir I, Taherzadeh S. Outdoor ground impedance models. J Acoust Soc Am 2011;129(5):2806–19.

[43] ANSI S1.18. Template method for ground impedance. American National Standards Institute, Acoustical Society of America; 1999.

[44] Bravo T, Ibarra D, Cobo P. Far-field extrapolation of maximum noise levels produced by individual vehicles. Appl Acoust 2013; 74:1463–72.

[45] Coleman TF, Li Y. An interior, trust region approach for nonlinear minimization subject to bounds. SIAM J Opt 1996; 6:418–45.

[46] Jesús, J., Aguilar, C., Antonio, J., Carrillo, C., Jesús, A., & Fernández, G. (2015). Robust Road Condition Detection System Using In-Vehicle Standard Sensors, 32056–32078.

[47] Wong, J.Y., Theory of Ground Vehicles, Wiley and Sons, 2001 (3rd edition)

[48] Jingang G., Xiaoping J. and Guangyu L. (2014) Performance Evaluation of an Anti-Lock Braking System for Electric Vehicles with a Fuzzy Sliding Mode Controller. Energies 2014, 7, 6459-6476.

[49] Autoriza, A., Uso, E. L., & Documento, D. E. E. (2003). Norma Española ISO 10534-2:1998.

[50] Turo, Diego. *Surface impedance, reflection and absorption coefficients measurements*. Report. Washington DC: The Catholic University of America, 2012. Document.

[51] IKA. *Linear Friction Measuring Device "LiReP"* . n.d. https://www.ika.rwth-aachen.de/en/research/equipment/testing-facilities/chassis/313-lirep-en.html. 20 10 2018.

[52] Masad, A. T. Papagiannakis and E. A. Pavement Design and Materials. New Jersey, USA: John Wiley & Sons, 2008. Printed.

[53] Astrom, C. G. Wallman & H. *Friction Measurement Methods and the Correlation between Road Friction and Traffic Safety: A Literature Review*. Linkoping, Sweden: Swedish national road and transport research institute, 2001. Document

[54] Byrd RH, Gilbert JC, Nocedal J. A trust region method based on interior point techniques for nonlinear programming. Math Programm 2000;89(1):149–85.

[55] Coleman TF, Li Y. An interior, trust region approach for nonlinear minimization subject to bounds. SIAM J Opt 1996; 6:418–45.

[56] Cobo P, Ortiz S, Ibarra D, de la Colina C. Point source equalised by inverse filtering for measuring ground impedance. Appl Acoust 2013; 74:561–5.

Abbreviations and Acronyms

Table A.1: Acronyms Definitions

Acronyms	*Description*	*Acronyms*	*Description*
ABS	Anti-lock Braking System	IRI	International Index of Roughness
ADAS	Advanced Driver Assistance System	PIARC	Permanent Intern. Assoc. of Road Congresses
IFI	International Friction Index	A.I.P.C.P.	American Inst. of Physics Conf. Proceedings
ITESM	Instituto Tecnológico de Monterrey	S.R.C.	Slip Resistance Coefficient
HMI	Human-Machine Interface	FR	Friction value
TDMS	Test Data Exchange Stream	TX	Texture value
LABVIEW	Lab. Virtual Instrument Engineering	ECU	Electronic Control Unit
DAQ	Data Acquisition	SPM	Small Perturbation Method
I/O	Input/output	FDTD	Finite-Difference Time-Domain
DAQ AI	Data Acquisition Analog Input	TLM	Transmission-Line Modeling
USA	United States of America	MLS	Maximum Length Sequence
LiReP	Linearzug-Reibwertprüfständ (GER)	MATLAB	Matrix Laboratory
LiReP	Linear Friction Measuring Device	PID	Proportional–Integral–Derivative
RNN	Recurrent Neural Networks	GND	Ground
IEEE	Institute of Electrical and Electronics	MIT	Massachusetts Institute of Technology
NIR	Near Infrared	SVM	Support Vector Machines

Variables Descriptions and Symbols

Table A.2: Variables and Symbols

Variable	*Description (units)*	*Variable*	*Description (units)*
s	Speed (m/s, km/h)	V	Volume (mm3)
d, D, Lc	Distance (m, km, mm)	ϕ	Diameter (mm)
f	Frequency (Hz)	π	Pi
F	Force (N)	TX	Texture (mm)
F_A	Force Adhesion (N)	FRs	British Pendulum Reading (dimensionless)
F_H	Force Hysteresis (N)	F60	Friction at 60 km/hr, (dimensionless)
μ	Coefficient of Friction	Sp	Macrotextures Sand Patch Value (km/h)
θ	Angular Displacement (°)	S	Velocity of British Pendulum (km/h)
I	Moment of Inertia	a	Acceleration (m/s2)
W	Weight (N)	F(s)	Friction for different speeds (dimensionless)
F_N	Normal Force (N)	R	Reflection Coefficient
BPN	British Pendulum Number	α	Acoustic Absorption Coefficient
h, H	Height (m, mm)	Z	Surface Impedance
P, p	Pressure (Pa)	*E, E**	Energy Flux (J)
Q	Spherical Wave Reflection coefficient	β	Surface Admittance
K_0	Wave vector	ξ(x)	High profile (m, mm)
C_0	Speed Sound (m/s)	L	Sound level (dB)
σ	Flow resistivity (Ns/m4)	φ	Porosity
T	Tortuosity	Sp	Shape Factor
m	Mass (kg, gr.)	ρ	Density (kg/mm3, gr/cm3)
Temp	Temperature (°C)	r	Correlation coefficient
t	Time (s, min, ms)	v, VCC	Voltage (V)
Ff	Friction Force (N)	g	Gravity acceleration (m/s2)
w	Angular Frequency (Hz)	λ_0	Wavelength (m)
Hc	Calibration Factor	S.R.C.	Slip Resistance Coefficient (dimensionless)
r_0	Air density (kg/m3)	r^2, R^2	Coefficient of determination

Appendix A

A.1 British Pendulum

Experimental procedure

The preparation of the device goes as following:

a) Leveling.

Level the instrument exactly (accurately) by turning the leveling screws until the bubble is centered in the eye leveling bubble.

b) Adjust to zeros.

The head of the apparatus is raised, so that the pendulum arm oscillates without touching the surface to be measured and the zero of the measuring scale is checked. To do this, the pendulum arm is brought to its horizontal position to the right of the device, being automatically hooked into the trigger mechanism. The indicator needle is then moved to the stop on the head of the device, so that it is parallel to the axis of the pendulum arm.

This stop, consisting of a screw, allows to correct the parallelism between the needle and the arm. Then, by pressing on the button, the pendulum arm is triggered, which will drag the indicator needle only in its oscillation forward. The reading indicated by the needle of the scale of the panel is denoted and the arm is returned to its initial firing position. The correlation of the zero reading is made by adjusting the friction rings. If the needle overpasses the zero of the scale, the correction will require tightening the friction rings. If the needle does not reach zero on the scale, the correction will require loosening the friction rings.

c) Adjustment of the sliding length.

With the pendulum hanging freely, place the spacing below the adjusting screw or adjustment of the pendulum arm. Lower the pendulum arm so that the surface of the rubber barely touches the surface. Block the pendulum head firmly, raise the pendulum arm, and remove the spacer. Place the gauge to the side and parallel to the direction of the roll to verify the length of the contact path.

Raise the pendulum arm, then gently lower it to the sliding surface again to rest or rest on the surface. If the length of the contact path is not between 124 and 127 mm (4 7/8 and 5.0 inches) on flat test surfaces or between 75 and 78 mm (2 15/16 and 3 1/16 of an inch) on surfaces test curves measured with the rubber, can be corrected by adjusting the pendulum lift or lower the instrument with the front leveling screws. [15]

Temperature correlation

The measurements made on the pavement are always affected by temperature variations of the rubber and the surface tested; therefore, a factor to the effective reading (FRs) is added to the

values obtained with the pendulum, as seen in Figure 46. For example, if an average reading of 78 was measured under a temperature of 30 ° C, a factor of 2 is added, giving a final value of 80.

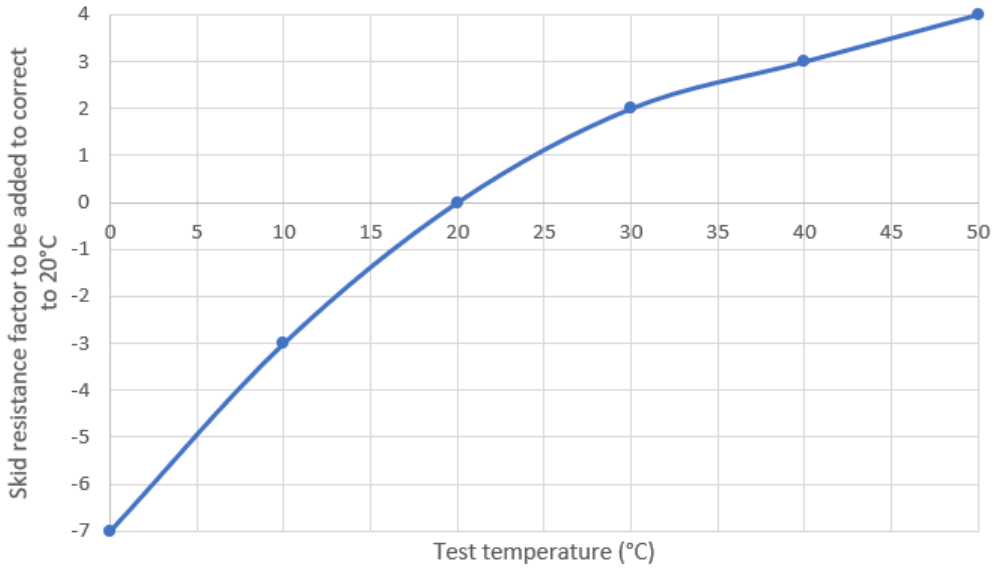

Figure 46 - Correction factor for temperature.

The results of the measurements made in each test area of a road section will be expressed by at least three values, corresponding to each one. Each one of the three values or more values obtained will be the arithmetic mean of all the readings made on the test points located in the considered surfaces and in all the cross sections of each section.

In pavements other than roadways, if no distribution of strips has been made, the result of the measurements made will be the value of the arithmetic mean of the readings made in each zone. [16]

A.2 Sand patch

Experimental procedure

The test procedure involves the dispersion of a known volume of material on a clean and dry pavement surface, the measurement of said covered area, and subsequently the average thickness is calculated between the lower part of the voids and the upper part of the aggregates. This measurement of the thickness of the surface texture reflects the characteristics of the macrotexture.

In the dispersion of the material specified in this method, the surface of the voids is filled up to the peaks of the surrounding particles. This test method is not considered suitable for use on fluted surfaces or pavements with large voids (≥ 1.0 in. (25mm)). [15]

Test surface. - Inspect the pavement surface for evaluation and select a dry and homogeneous area that does not contain unique or localized features such as cracks and joints. It must be completely clean using first the wire brush and then the soft bristle brush to remove any residue, debris or loose aggregate particles from the surface. Place the wind screen around the surface to be tested.

Test material. - Fill the volume of known material with dry material, gently tap the base of the cylinder several times on a rigid surface. Fill with material to the top of the cylinder and level with a strip. If a balance is available, determine the mass of the material in the cylinder in the cylinder and use this same mass of test material in each determination.

Measurement of the assay. - Pour the volume of material on the clean surface into the area protected by the wind screen. Carefully disperse the material in the circular patch with the disc tool, with the part covered with rubber down, filling the surface voids up to the peaks of the aggregate particles.

Measure and record the diameter of the area covered by the material at least four equally spaced locations around the circumference of the sample. Calculate and record the average diameter.

Number of test measurements. - The same operator must develop at least four measurements of the thickness of the macrotexture, randomly spaced over a type of pavement surface tested. The arithmetic average of the thickness values of the macrotexture should be considered as the average thickness of the macrotexture of the surface of the pavement under study. [18]

Equipment

Material. - Spheres of solid glass with 90% roundness according to the test method ASTM D 1155 or graded sand could be used in such a way that they have a minimum of 90% by weight that passes the No. 60 mesh and is retained in a No. 80.

Test container. - A cylindrical metal or glass container with a predetermined internal volume of at least 1.5 cubic inches (25,000 mm3) can be used, which will be used to determine the volume of dispersed sand.

Scattering tool. - A flat hard disk about 1 inch (25 mm) thick and 2.5 to 3 inches (60 to 75 mm) in diameter should be used to disperse the sand. The bottom of the disc should be covered with a hard rubber material and a convenient handle can be attached to the top of the disc. Or if this tool is not available, it can be replaced by a ruler, long enough to cover the diameter formed by the scattered sand.

Brushes. - A wire brush and a soft bristle brush should be used to completely clean the pavement surface before application of the test material.

Screen against wind. - It is used to protect wind material and turbulence created by traffic.

Scale. - A standard scale (ruler or tape measure) of 12 in. Should be used. (305 mm) or longer length containing divisions of 0.1 in. (2.5mm) or 1mm (0.04 in.).

Use a laboratory scale, with sensitivity of 0.1 g, it is recommended with this test method to provide additional control and to ensure that the amount of material used for each measurement of the thickness of the macrotexture is equal in both mass and volume.

Appendix B

GUI of Data Acquisition System

A MATLAB Graphical User Interface (GUI) was used to acquire and to identify the characteristics of the ground surface measured according with a variant of the ANSI S1.18 standard.

Its implementation allows selecting the values for the position of the source and receivers, and the atmospheric conditions. Impedance models are considered with a surface's configuration of homogeneous layers and with local reaction. The user interface allows plotting the level difference between the two sensors, the windowed original signal and a theoretical curve fitted to the experimental curve according to the geometrical set up, and values of one, two, three and four parameters as a result.

Figure 60 shows the home window of the Graphical User Interface (GUI), which is a useful tool to facilitate the measurement and characterization of the ground surface and extract important parameters. The application is simple and functional, as it provides the necessary options to select from 1 to 4 of the parameters, allowing the user to enter data regarding the location of the sound source and receivers, as the experimental curve needs to be compared with the theoretical curves in the same geometrical arrangement.

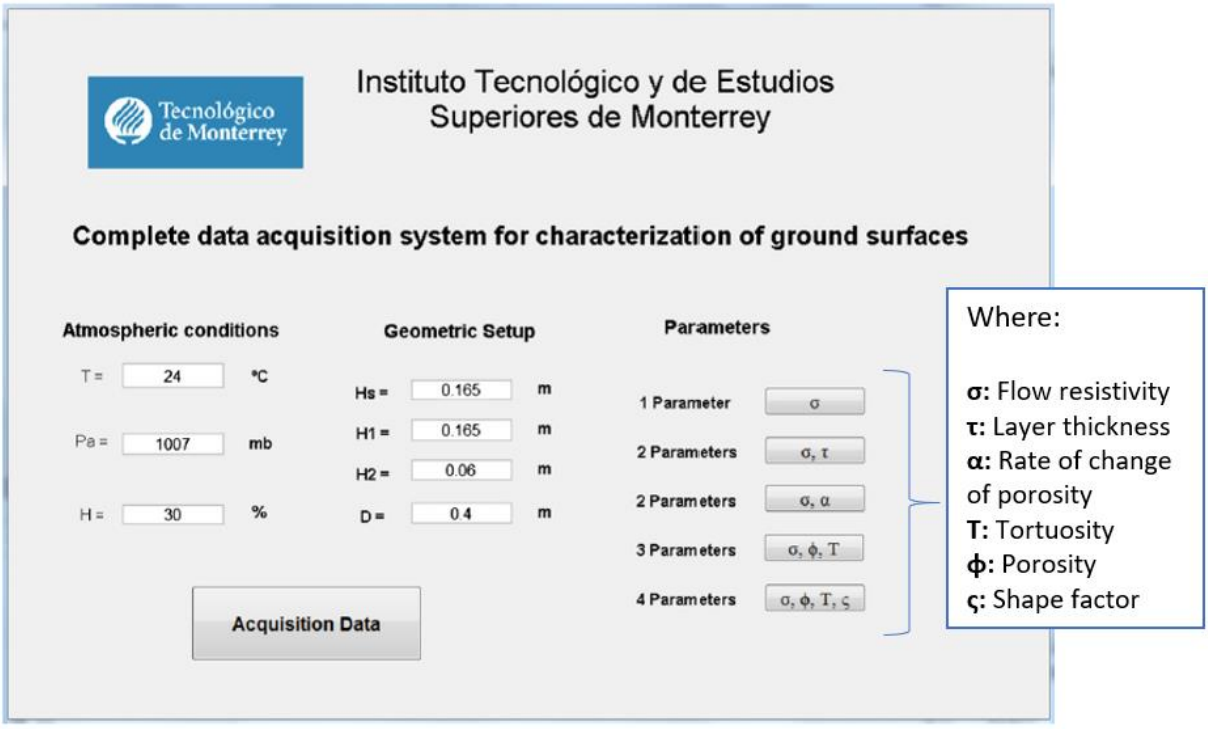

Figure 47 - Matlab Graphical User Interface (GUI)

Weather conditions are also important, since the determination of sound propagation requires information on temperature, relative humidity and barometric pressure as a function of height near the propagation path. These values determine the sound speed profile.

In the right-hand part of Fig. 60, the impedance model can be selected, depending on how many parameters are required. For example, one parameter: flow resistivity σ; two parameters: flow resistivity σ and layer thickness τ; two parameters: flow resistivity σ and rate of change of porosity α; three parameters: flow resistivity σ, porosity φ and tortuosity T; and four parameters: flow resistivity σ, porosity φ, tortuosity T and shape factor ς. To start the measurement the acquisition data button is pressed, and the results can be obtained in less than 5 s.

In order to make the comparison and adjustment between the experimental and theoretical curves, a code in Matlab was implemented, establishing all the ranges for each parameter under test, and a nonlinear programming that attempts to find a constrained minimum of a scalar function of several variables starting at an initial estimate [54]. This is generally referred to as constrained nonlinear optimization [55].

The frequency fitting range for comparing the theoretical curves, for this case is 1–5 kHz, due to the absorption and reflection in the path. As an example, in Figure 61 the final result shows the 4 parameters, in the case of a speed of 20 km/h: σ = 0.78 106 N s/m4, φ = 0.9, T = 1 and ς = 0.42; the result in the GUI plots the original signal windowed (blue) and the theoretical (red) curve, displaying minor discrepancies between them. In all the cases a temporary window in both signals (top and bottom microphones) to eliminate the unwanted reflections incoming from close obstacles and decrease the background noise was applied.

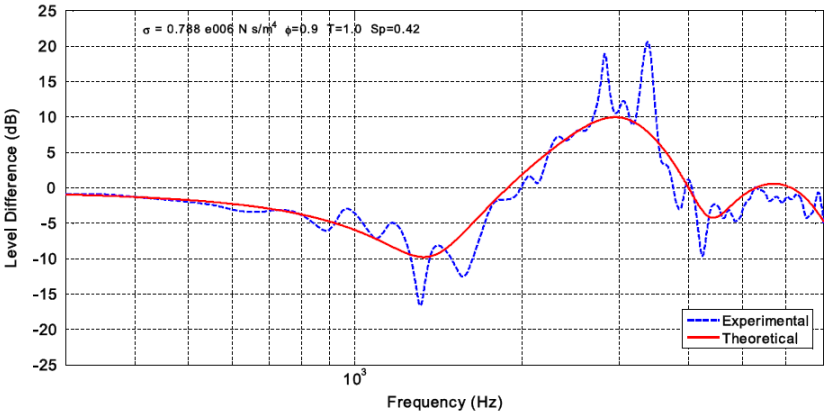

Figure 48 – Theoretical and experimental level difference curves for the asphalt at 20 km/h

Fig. 62 shows another final result, using 4 parameters; in this case, a speed of 100 km/h, σ = 0.78 106 N s/m4, φ = 0.68, T = 5.8 and ς = 0.45. The result in the GUI plots the original signal windowed (blue) and the theoretical (pink) curve displaying minor differences between them.

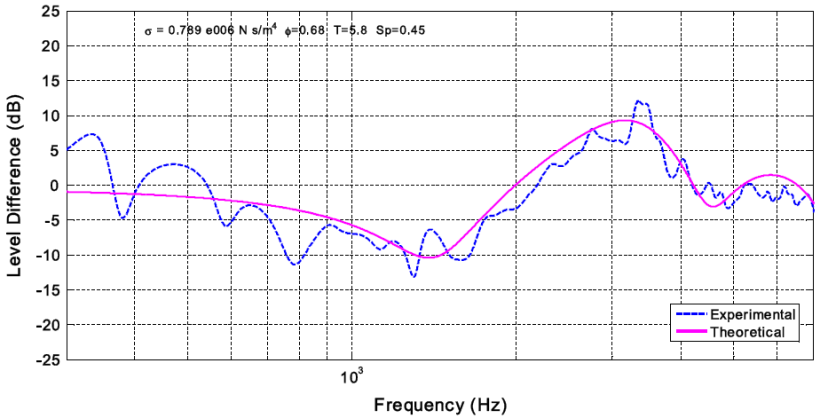

Figure 49 - Theoretical and experimental level difference curves for the asphalt at 100 km/h

In all the cases a temporary window was applied in both signal (top and bottom microphones) to eliminate the unwanted reflections incoming from close obstacles and decrease the background noise [56].

Appendix C

Impedance Tube

Basic principle of measurements performed with an impedance tube

An impedance tube is a straight, rigid, smooth cylindrical pipe composed by two main sections or tubes: transmitting and receiving tube. The test sample is mounted at one end of the impedance tube (receiving tube). Plane waves are generated in the transmitted tube by a sound source (random, pseudo-random sequence, or chirp), and the sound pressures are measured at two locations near to the sample (preferably less than 3 times the diameter of the tube). The complex acoustic transfer function of the two microphone signals is determined and used to compute the normal-incidence complex reflection coefficient $R(\omega)$, the normal-incidence absorption coefficient $\alpha(\omega)$, and the surface impedance of the test material $Zs(\omega)$. [49]

The quantities are determined as functions of the frequency with a frequency resolution which is determined from the sampling frequency and the record length of the digital frequency analysis system used for the measurements. The usable frequency range depends on the width of the tube and the spacing between the microphone positions.

The measurements may be performed by employing one of two following techniques:

1. two-microphone method (using two microphones in fixed locations);
2. one-microphone method (using one microphone successively in two locations).

Technique 1 requires a pre-test or in-test correction procedure to minimize the amplitude and phase difference characteristics between the microphones; however, it combines speed, high accuracy, and ease of implementation. This technique is recommended for general test purposes.

Technique 2 has signal generation and processing requirements and may require more time; however, it eliminates phase mismatch between microphones and allows the selection of optimal microphone locations for any frequency. It is recommended for precision.

For main purpose the technique 2 was used on the experimentation.

Acoustic characteristics and surface impedances

The acoustic impedance at a frequency indicates how much sound pressure is generated by the

vibration of molecules of an acoustic medium at a given frequency. [50]

The ratio of acoustic pressure in a medium to the associated particle velocity is defined as specific impedance (or surface impedance if referred to an interface between two fluids or fluid-solid):

$$Z_s = \frac{p(x,t)}{v(x,t)} \tag{25}$$

It is usually a complex quantity. However, it is a real quantity for progressive plane waves (because pressure and particle velocity are in phase).

$$Z_s = \frac{p(x,t)}{v(x,t)} = \frac{j\omega\rho_0 cA(\omega)e^{j(\omega t-kx)}}{j\omega A(\omega)e^{j(\omega t-kx)}} = \rho_0 c = Z_c \tag{26}$$

The product of the fluid density by the speed of sound in that fluid, $\rho_0 c$, defines a characteristic property of the medium and therefore is often called characteristic impedance. For standing plane waves and diverging waves specific impedance is a complex quantity.

Superposition of two waves propagating in opposite directions

The pressure and the velocity, for a wave propagating toward the positive abscissa are, respectively,

$$p(x,t) = Ae^{j(-kx+\omega t)} \tag{27}$$

$$v(x,t) = \frac{A}{Z_c}e^{j(-kx+\omega t)} \tag{28}$$

The pressure and the velocity, for a wave propagating toward the negative abscissa are, respectively,

$$p^*(x,t) = A^*e^{j(kx+\omega t)} \tag{29}$$

$$v^*(x,t) = -\frac{A^*}{Z_c}e^{j(kx+\omega t)} \tag{30}$$

If the acoustic field is a superposition of the two waves described by the above equations, the total pressure $p_T(x,t)$ and the total velocity $v_T(x,t)$ are:

$$p^*(x,t) = A^*e^{j(kx+\omega t)} \tag{31}$$

$$v^*(x,t) = -\frac{A^*}{Z_c}e^{j(kx+\omega t)} \tag{32}$$

A superposition of several waves of the same ω and k propagating in a given direction is equivalent to one resulting wave propagating in the same direction. The ratio $p_T(x,t)/v_T(x,t)$ is

called the impedance at x.

Impedance variation along a direction of propagation

In Figure 47, two waves propagate in opposite directions parallel to the x-axis. The impedance $Z(x_2)$ at x_2 is known. The impedance $Z(x_2)$ can be written:

$$Z(x_2) = \frac{p_T(x_2,t)}{v_T(x_2,t)} = Z_c \frac{Ae^{j(-kx_2+\omega t)} + A^* e^{j(kx_2+\omega t)}}{Ae^{j(-kx_2+\omega t)} - A^* e^{j(kx_2+\omega t)}} = Z_c \frac{Ae^{j(-kx_2)} + A^* e^{j(kx_2)}}{Ae^{j(-kx_2)} - A^* e^{j(kx_2)}} \tag{33}$$

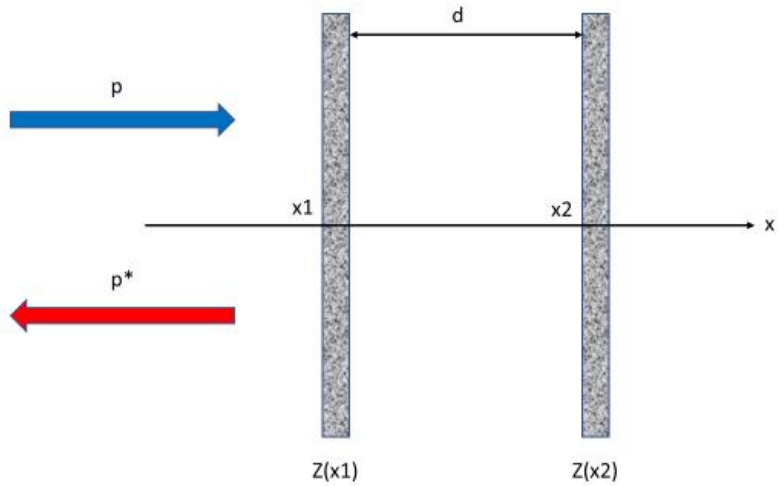

Figure 50 - Layer of fluid.

Whereas at x_1, the impedance $Z(x_1)$ can be written:

$$Z(x_1) = \frac{p_T(x_1,t)}{v_T(x_1,t)} = Z_c \frac{Ae^{j(-kx_1)} + A^* e^{j(kx_1)}}{Ae^{j(-kx_1)} - A^* e^{j(kx_1)}} \tag{34}$$

From the above equations one can evaluate the following expression:

$$\frac{A}{A^*} = \frac{Z(x_2) - Z_c}{Z(x_2) + Z_c} e^{-2j(kx_2)} \tag{35}$$

which gives:

$$Z(x_1) = Z_c \frac{-jZ(x_2)\cot(kd) + Z_c}{Z(x_2) - jZ_c \cot(kd)} \tag{36}$$

where d is equal to $x_2 - x_1$. The above equation is known as the impedance translation theorem.

Impedance at normal incidence of a layer of fluid backed by an impervious rigid wall

As shown in Figure 48, a layer of fluid 2 is backed by a rigid plane of infinite impedance at $x_2 = 0$ as shown in in the figure below. The impedance at x_1 at the surface of the layer of fluid 2 is obtained from:

$$Z(x_1) = \lim_{Z(x_2)\to\infty}\left[Z_c \frac{-jZ(x_2)\cot(kd) + Z_c}{Z(x_2) - jZ_c\cot(kd)}\right] = Z_c \frac{-jZ(x_2)\cot(kd)}{Z(x_2)} = -jZ_c\cot(kd) \qquad (37)$$

where Z_c is the characteristic impedance and k the wave number in fluid 2.

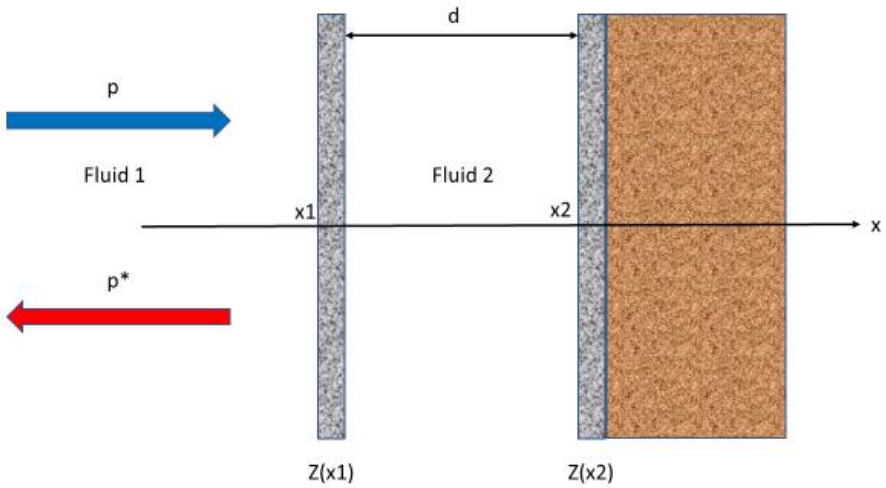

Figure 51 - Layer of fluid backed by a rigid wall

The pressure and the velocity are continuous at the boundary. The impedance at both sides of the boundary are equal, the velocities and pressures being the same on either side of the boundary.

Impedance at normal incidence of a multilayered fluid

The impedance of a multilayered fluid can be easily evaluated applying the previous equations layer by layer. Starting from a known impedance at $x_n = 0$, $Z(x_{n-1})$ is evaluated and used as know impedance for the next layer and so on.

Reflection coefficient and absorption coefficient at normal incidence

Reflection coefficient

The reflection coefficient R at the surface of a layer is the ratio of the pressures p^* and p created by the outgoing and the ingoing waves at the surface of the layer. For instance, at x_1, in Figure 48, the reflection coefficient $R(x_1)$ is equal to:

$$R(x_1) = \frac{p^*(x_1, t)}{p(x_1, t)} \tag{38}$$

This coefficient does not depend on t because the numerator and the denominator have the same dependence on t. Using previous equations, the reflection coefficient $R(x_1)$ can be written as:

$$R(x_1) = \frac{Z(x_1) - Z_{c1}}{Z(x_1) + Z_{c1}} \tag{39}$$

where Z_{c1} is the characteristic impedance in fluid 1. The ingoing and outgoing waves at x_1 have the same amplitude if $|R(x_1)| = 1$. This occurs if $|Z(x_1)|$is infinite or equal to zero. If $|Z(x_1)|$ is greater than 1, the amplitude of the outgoing wave is larger than the amplitude of the ingoing wave. More generally, the coefficient R can be defined everywhere in a fluid where an ingoing and an outgoing wave propagate in opposite directions.

Absorption coefficient

The absorption coefficient $a(x_1)$ is related to the reflection coefficient $R(x_1)$ as follows:

$$a(x_1) = 1 - |R(x_1)|^2 \tag{40}$$

The phase of $R(x_1)$ is removed, and the absorption coefficient does not carry as much information as the impedance or the reflection coefficient. The absorption coefficient is often used in architectural acoustics, where this simplification can be advantageous. It can be rewritten as:

$$a(x_1) = 1 - \frac{E^*(x_1)}{E(x_1)} \tag{41}$$

where $E(x_1)$ and $E^*(x_1)$ are the average energy flux through the plane $x = x_1$ of the incident and the reflected waves, respectively.

Appendix D

Experimentation with Impedance tube

The first part of the experimentation consists in measuring the friction coefficient (μ) of asphalt sample tests with the British pendulum. Afterwards, the acoustic absorption (α) is going to be obtained by using the Impedance tube.

A comparison between both mechanical and acoustical methods for asphalt characterization is going to be then evaluated.

D.1 Granulometric composition of experimental samples

With a final amount of 6,000 gr of material generated per batch, 2 sample tests of 2,500 gr each are created. For the experimentation 4 different batches with variation on the asphalt content were created. At Table 13 it is possible to observe the quantities of material passing through the mesh in individual and accumulated amounts per batch.

Table 13 – Granulometry of experimental tests per batch

				Accumulated	
Mesh	Limestone (gr)	Granite (gr)	% Passes	Limestone (gr)	Granite (gr)
1/2	177.5	95.5	95.5	177.5	4723.3
3/8	1343.6	723.5	61	1521.1	5446.8
4	1027.7	553.4	34.7	2548.8	6000.2
10	915		19.4	3463.8	
20	405		12.7	3868.8	
40	30		12.2	3898.8	
60	15		11.9	3913.8	
100	39		11.3	3952.8	
200	15		11	3967.8	
Finos	660			4627.8	
Individual Weight (gr)	4627.8	1372.4			
Total Weight (gr)	6000.2				

The tests created were composed of asphalt 76-22, at 160 turns, a rotary compaction of 600 kPa and 170°C, with a composition of 35% granite and the rest of limestone.

At Table 14 the characteristics of height, weight, density and percentage of asphalt for the different test samples are shown.

Table 14 – Asphalt 76-22 test sample properties

Test	Height (mm)				Weight (gr)			Density (gr/cm3)		%
#	h1	h2	h3	h ave	Dry	Submerged	SS	Apparent	Submerged	Asphalt
T1	62.0	61.0	62.0	61.67	2612.1	1532.1	2617.8	2.322	2.406	5.0
T2	63.0	63.0	63.0	63.00	2614.9	1525.8	2620.6	2.275	2.388	
T3	64.2	64.2	64.1	64.17	2605.8	1522.7	2615.9	2.226	2.384	4.5
T4	65.0	65.2	65.0	65.07	2606.2	1516.5	2616.0	2.196	2.370	
T5	63.6	63.6	63.7	63.63	2613.6	1536.5	2617.4	2.252	2.418	5.5
T6	63.5	63.6	63.7	63.60	2612.9	1533.4	2616.8	2.252	2.412	
T7	66.4	66.7	67.0	66.70	2624.8	1513.4	2631.2	2.157	2.348	6.0
T8	65.0	65.1	65.0	65.03	2608.4	1517.1	2612.8	2.199	2.381	

Figure 49 shows the test samples created at the laboratory; divided in groups of two according to the asphalt percentage (4.5, 5, 5.5 and 6%).

Figure 52 – Sample tests divided by percentage of asphalt 76-22.

D.2 Experimental Measurements

D.2.1 British Pendulum

Figure 50 shows the Pendulum with the four different test samples to be measured at the laboratory of asphaltic materials, and Table 15 shows the results of the corresponding friction coefficients at a controlled room temperature of 20.4 °C after water was applied.

Figure 53 - British pendulum measurement experimentation

Table 15 - Friction values measured with the British Pendulum on test samples

	T2	T3	T6	T8
Average FRs	0.544	0.64	0.6	0.574
Temperature (°C)	20.4	20.5	20.4	20.1
Skid resistance factor	0	0	0	0
Friction (S.R.C)	**0.544**	**0.64**	**0.6**	**0.574**

D.2.2 Impedance Tube

Figure 51 show the experimental measurements made with the Impedance tube with the objective of obtaining the acoustic properties of the test samples. For information about the calibration of the measurement setup, please refer to Appendix E.

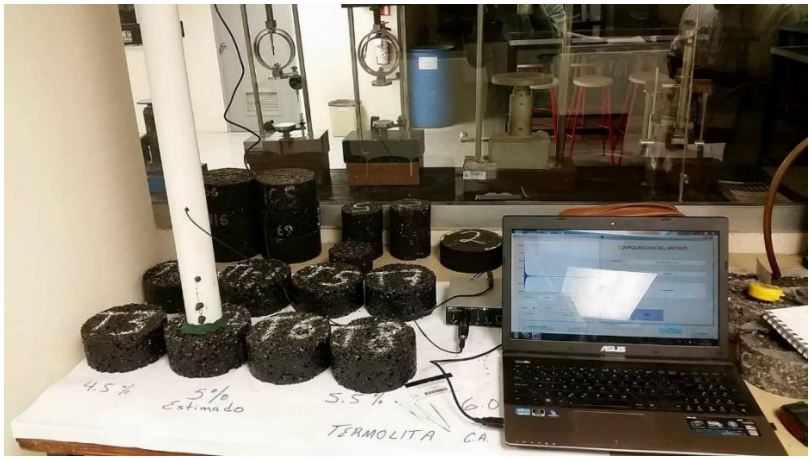

Figure 54 – Analysis of measurements using MATLAB

The normal incidence sound absorption coefficient is given by the following equation:

$$a(w) = 1 - |R|^2 \tag{42}$$

After processing the data tests using Matlab, the graph of the absorption coefficients of the four sample tests is found in Figure 52 for a frequency range between 700 and 1100 Hz.

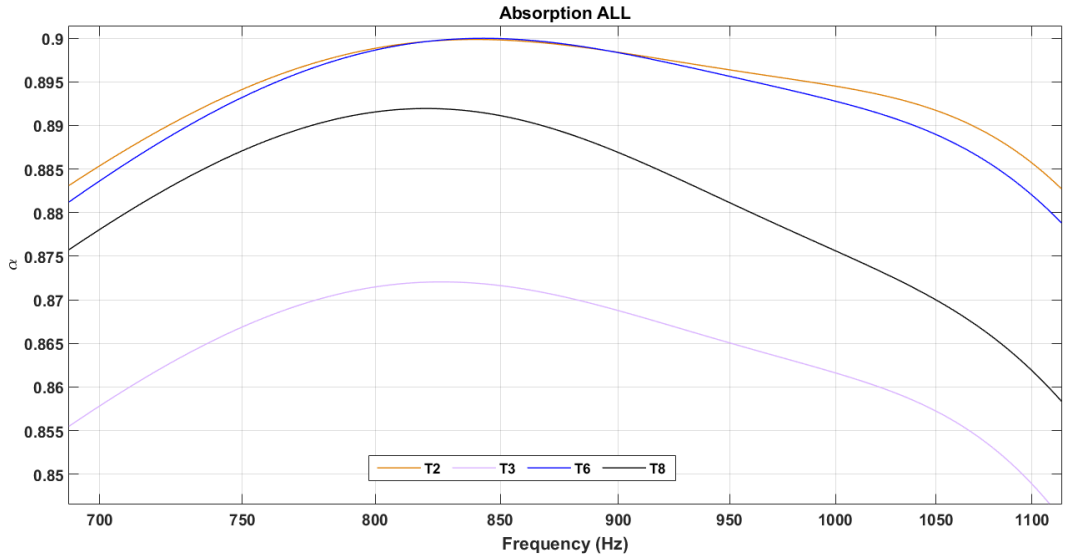

Figure 55 – Acoustic absorption comparison between 700-1100 Hz

Table 16 shows the acoustic absorption values obtained with the impedance tube for a selective number of frequencies (700-1100 Hz). It was decided to work and analyze between this range of frequencies because here is where the highest absorption and stability values are presented.

Table 16 – Acoustic absorption (α) values for different frequencies

	Frequency (Hz)				
	700	**800**	**900**	**1000**	**1100**
T2	0.885	0.899	0.898	0.895	0.885
T3	0.858	0.872	0.869	0.862	0.849
T6	0.883	0.899	0.898	0.893	0.882
T8	0.878	0.892	0.887	0.875	0.862

D.3 Results

Figure 53 to 57 show the linear correlation between the Friction (S.R.C.) and the acoustic absorption coefficient (α) for different frequency values, where the linear regression equation (y) and the coefficient of determination (r^2) are also displayed on the graphs.

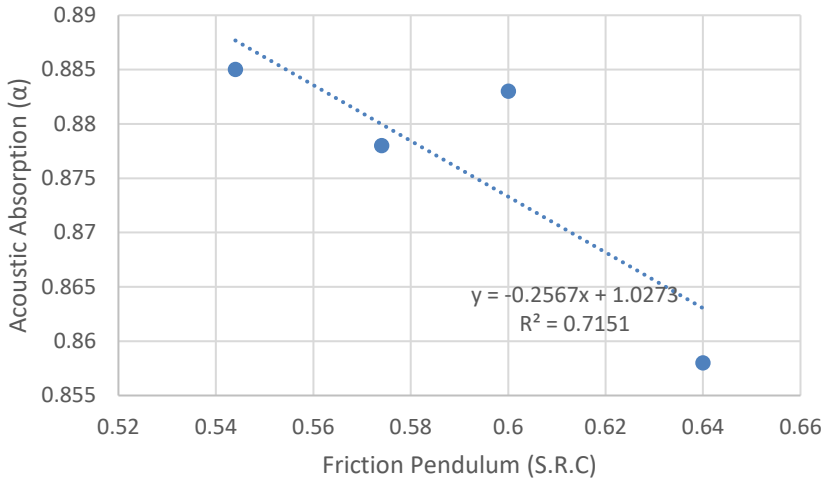

Figure 56 – Friction vs Ac. Absorption for 700 Hz

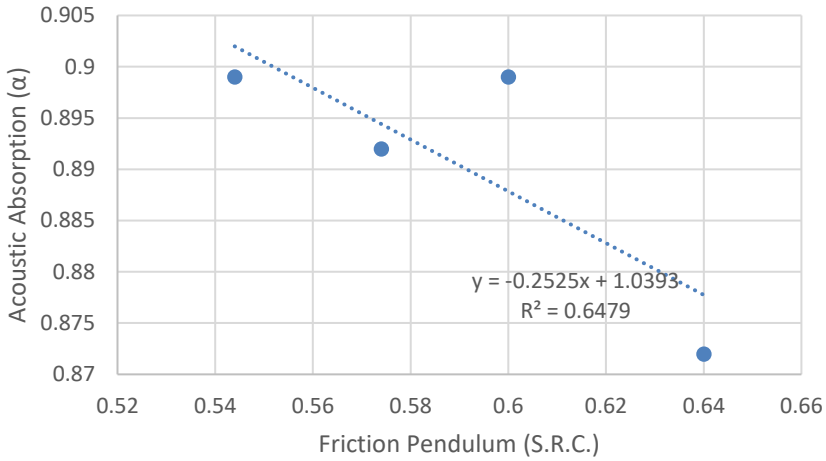

Figure 57 – Friction vs Ac. Absorption for 800 Hz

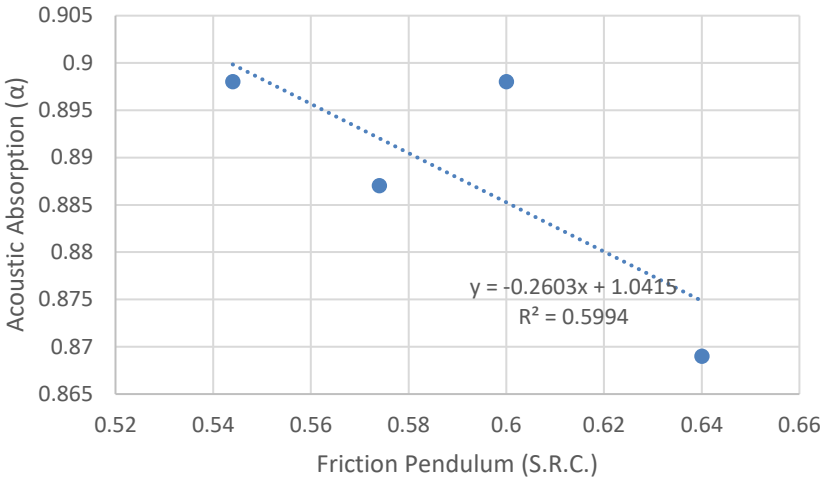

Figure 58– Friction vs Ac. Absorption for 900 Hz

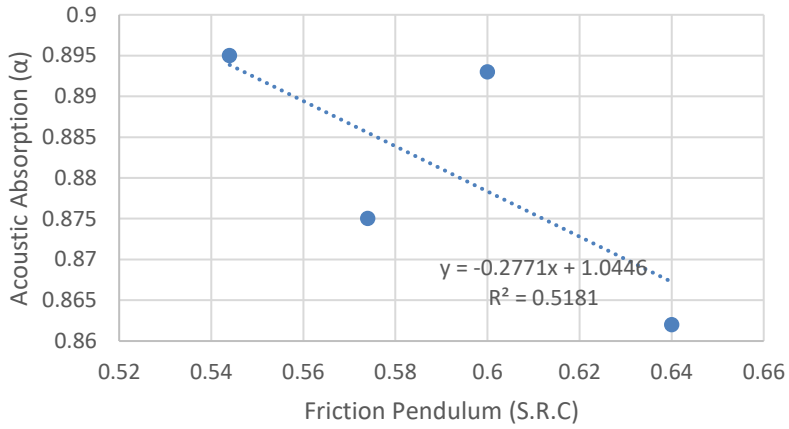

Figure 59 – Friction vs Ac. Absorption for 1000 Hz

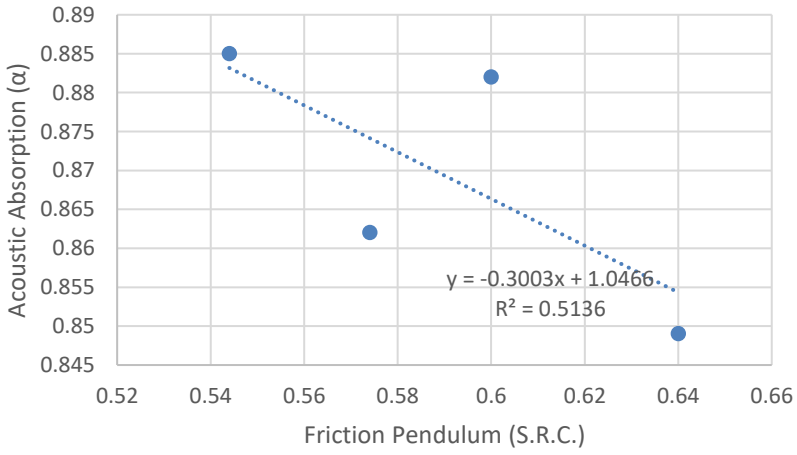

Figure 60 – Friction vs Ac. Absorption for 1100 Hz

D.4 Discussion

Original hypothesis:

- $\alpha \rightarrow 1$ = The most acoustic absorption; the most porosity, the least density, the most flux resistivity, the most friction, and the most adhesion to pavement available.
- $\alpha \rightarrow 0$ = The least acoustic absorption; the least porosity, the most density, the least flux resistivity, the least friction, and the least adhesion to the pavement available.

By looking back at the original hypothesis, at the beginning it was thought that the higher acoustic absorption coefficient (α), the higher coefficient of friction (μ) obtained, but the results showed the opposite. Instead, it is seen that the higher the acoustic absorption, the lower the friction available.

Furthermore, very strong negative correlation coefficients were obtained for the different frequencies analyzed, as seen in Table 17:

Table 17 – Acoustic vs. Friction correlation coefficient for different frequencies

Frequency (Hz)	Correlation Coefficient (r)
700	-0.8456
800	-0.8049
900	-0.7742
1000	-0.7198
1100	-0.7166

That is why, it is concluded that after the first experimentation with the impedance tube, there is a good reason to believe that the acoustic characterization could be used as a valid method to characterize the road surface. The next step will be to make more measurements on the field to obtain more data for comparison.

Appendix E

Calibration of impedance

tube measurement setup

Selection of the signal amplitude

The signal amplitude must be at least 10 dB higher than the background noise at all frequencies of interest, as measured at the chosen microphone locations. During a test, any frequency having a response value 60 dB lower than the maximum frequency response value must be rejected. [50]

Correction for microphone mismatch

When using the two-microphone technique, one of the following procedures for correcting the measured transfer function data for channels mismatch must be used: repeated measurements with channels interchanged, or predetermined calibration factor. A channel consists of a microphone, preamplifier and analyzer channel.

Measurement repeated with the microphones interchanged

Correction for microphone mismatch is done by interchanging channels for every measurement on a test specimen. This procedure is highly preferred when a limited number of specimen are to be tested. Place the test specimen in the tube and measure the two transfer functions $H_{12}^{I}(w)$ and $H_{12}^{II}(w)$, using the same mathematical expressions for both. Place the microphones in configuration I (standard configuration, see Figure 58) and store the transfer function $H_{12}^{I}(w)$. Interchange the two microphones A and B.

When interchanging the microphones, ensure that microphone A in configuration II (microphones interchanged, see Figure 59) occupies the precise location that microphone B occupied in configuration I (standard configuration), and *vice versa*. Do not switch microphone connections to the preamplifier or signal analyzer.
Measure the transfer function $H_{12}^{II}(w)$ and compute the transfer function using equation:

$$H_{12}(w) = \sqrt{H_{12}^{I}(w) H_{12}^{II}(w)} = |H_{12}| e^{jf} \tag{43}$$

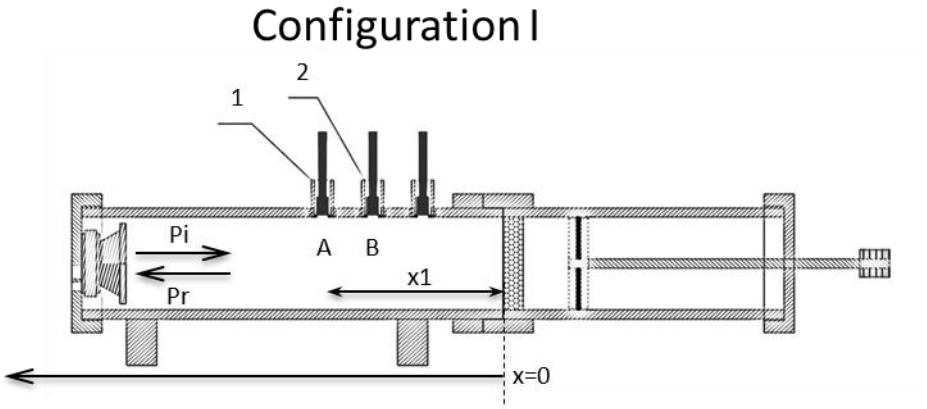

Figure 61 - Impedance tube configuration I: microphone A in position 1 and microphone B in position 2.

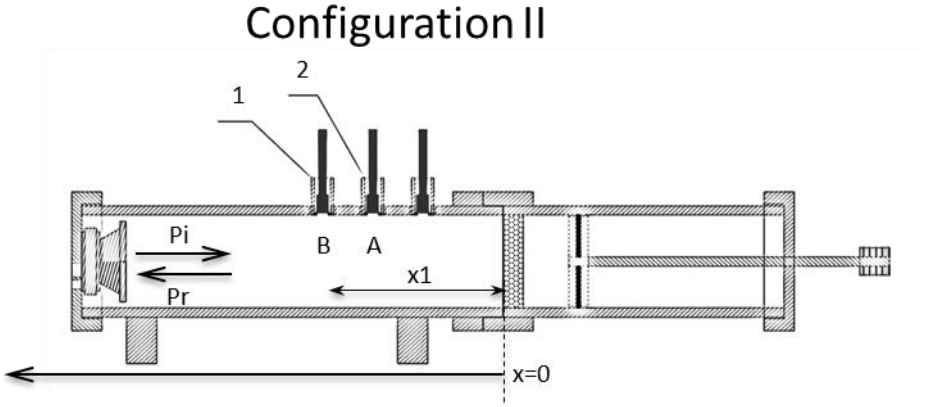

Figure 62 - Impedance tube configuration II: microphone B in position 1 and microphone A in position 2.

If the analyzer is only able to measure transfer functions in one direction (e.g from microphone A to microphone B), $H_{12}(w)$ can be computed using:

$$H_{12}(w) = \sqrt{\frac{H_{12}^{I}(w)}{H_{21}^{II}(w)}} = |H_{12}|e^{jf} \tag{44}$$

Calibration factor

The calibration procedure uses a special calibration specimen and the correction is valid for all successive measurements. This procedure is performed once and after calibration the microphones remain in place.

Place an absorptive specimen in the tube to prevent strong acoustic reflections and measure the two transfer functions $H_{12}^{I}(w)$ and $H_{12}^{II}(w)$.

Compute the calibration factor using the following expression:

$$H_{c}(w) = \sqrt{\frac{H_{12}^{I}(w)}{H_{12}^{II}(w)}} = |H_{c}|e^{jf} \tag{45}$$

or, if the analyzer is only able to measure transfer functions in one direction (e.g from microphone A to microphone B), $H_c(w)$ can be computed using:

$$H_c(w) = \sqrt{H_{12}^{I}(w) H_{21}^{II}(w)} = |H_c| e^{jf} \tag{46}$$

For subsequent tests, place the microphones in configuration I (standard configuration). Insert the test specimen and measure the transfer function:

$$\hat{H}_{12}(w) = |\hat{H}_{12}| e^{j\hat{f}} = \mathrm{Re}(\hat{H}_{12}) + j\,\mathrm{Im}(\hat{H}_{12}) \tag{47}$$

where

$\hat{H}_{12}(w)$ is the uncorrected transfer function and $\hat{f}$ is the uncorrected phase angle;

Correct for mismatch in the microphone responses using the following equation:

$$H_{12}(w) = |H_{12}| e^{jf} = \frac{\hat{H}_{12}(w)}{H_c(w)} \tag{48}$$

Annex A

Construction of the Impedance tube

As seen on paper [49], the steps to build the impedance tube according to ISO 10534-2: 1998 were followed, as seen in Figures 60 and 61.

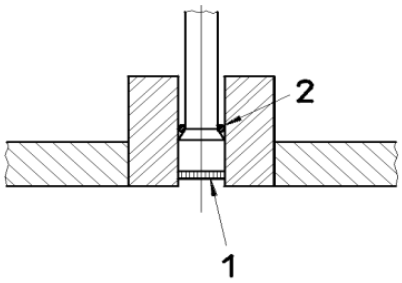

Legend:
1) Microphone
2) Sealing

Figure 63 – Example of microphone assembly. [49]

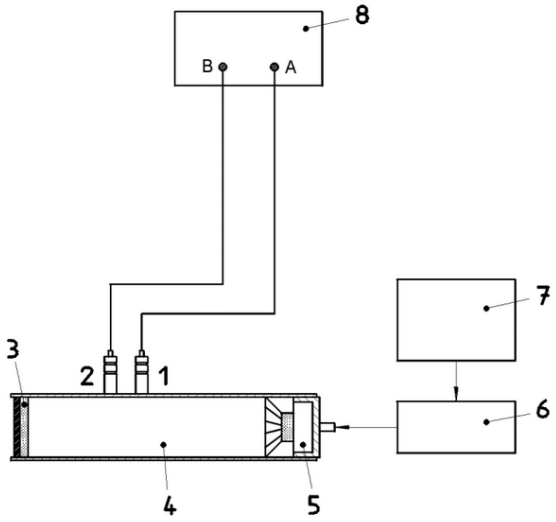

Legend:
1) 1st microphone placement
2) 2nd microphone placement
3) Test sample
4) Impedance tube
5) Acoustic source
6) Amplifier
7) Signal generator
8) Frequency analysis system

Figure 64 – Example of system assembly. [49]

Curriculum Vitae

Name: Jesús Rodrigo Leos Suárez

Date of birth: 26.01.1993

Place of birth: Chihuahua, Mexico

STUDIES

01/2017 – 12/2018	**Studies of M. Sc. Manufacturing Systems** at Instituto Tecnológico de Estudios Superiores de Monterrey (ITESM); in Monterrey, Mexico.
06/2018 – 11/2018	**IKA – RWTH Aachen University, Aachen** Research assistant and writing of the master thesis. In charge of the automation of the LiReP, device for measuring the friction of the pavement.
08/2011 – 12/2016	**B.S. Automotive Engineering** at Instituto Tecnológico de Estudios Superiores de Monterrey (ITESM); in Monterrey, Mexico.
05/2016 – 07/2016	**McMaster University, Canada** Research assistant, in charge of the design and manufacture of an Automated Guided Vehicle.
08/2014 – 08/2015	**Scholarship from the DAAD** to study at the "Technische Hochschule Ingolstadt", Germany, at the Faculty of Automotive Engineering.
08/2008 – 05/2011	**High school** at Prepa Tec Eugenio Garza Lagüera (CEGL) with an additional degree in Robotics and Computer Systems, in Monterrey.

This document was typed in using WORD by Jesús Rodrigo Leos Suárez.